INVESTIGATION OF FRICTION STIR BACK EXTRUSION

by

Obadah Mosbah Al-Jarrah

A Thesis Presented to the Faculty of the
American University of Sharjah
College of Engineering
in Partial Fulfillment
of the Requirements
for the Degree of

Master of Science in
Mechanical Engineering

Sharjah, United Arab Emirates

January 2020

Approval Signatures

We, the undersigned, approve the Master's Thesis of Obadah Mosbah Al-Jarrah.

Thesis Title: Investigation of Friction Stir Back Extrusion

Signature	**Date of Signature** (dd/mm/yyyy)
_____	_____
Dr. Mohammad Nazzal Associate Professor, Department of Mechanical Engineering Thesis Advisor	
_____	_____
Dr. Bassil Darras Associate Professor, Department of Mechanical Engineering Thesis Co-Advisor	
_____	_____
Dr. Maen Alkhader Associate Professor, Department of Mechanical Engineering Thesis Committee Member	
_____	_____
Dr. Mohammad AlHamaydeh Professor, Department of Civil Engineering Thesis Committee Member	
_____	_____
Dr. Mamoun Abdel-Hafez Head, Department of Mechanical Engineering	
_____	_____
Dr. Lotfi Romdhane Associate Dean for Graduate Affairs and Research College of Engineering	
_____	_____
Dr. Naif Darwish Acting Dean, College of Engineering	
_____	_____
Dr. Mohamed El-Tarhuni Vice Provost for Graduate Studies	

Acknowledgement

I would like to thank my advisors Dr. Mohammad Nazzal and Dr. Basil Darras for providing knowledge, guidance, support, and motivation throughout my research stages. I'm deeply beholden for their great assistance, worthy discussion and suggestions.

I would like to pay my special regards to the American University of Sharjah for helping and providing me with a graduate assistantship to complete my studies.

A special thanks to my family. Words cannot express how grateful I am to my mother, father, and brothers for all of the sacrifices that you have made on my behalf. Your prayer for me was what sustained me thus far. I would also like to thank to my beloved wife, Saja Mhmoud. Thank you for supporting me for everything, and especially I cannot thank you enough for encouraging me throughout this experience.

Abstract

Friction Stir Back Extrusion (FSBE) is a new bulk deformation manufacturing process that utilizes severe plastic deformation to force the processed material to produce a tubular shape. To date, most of the research conducted in the field of FSBE investigates the mechanical behavior of the produced tubes without paying enough attention to the temperature history, strain rates or the material flow during deformation. In this work, a multiphysics thermomechanical model based on the coupled Eulerian Lagrangian approach was developed to simulate the FSBE process and investigate the material flow, strains, strains rates, grain size and temperature history in the formed tube during deformation. The numerical model accounts for large plastic deformation, heat generation due to friction and plastic deformation, tool-workpiece and die-workpiece mechanical and thermal interaction to accurately simulate the FSBE process. FSBE experiments for Mg AZ31 alloy were conducted to validate the numerical FSBE model. It is shown that the reactive body force in the principal loading direction and the temperature history in the die obtained from numerical modeling agree well with experiments. The numerical results show that strain rates in the range of 70 s^{-1} were attained at the inner surface of the formed tubes. The maximum temperature in the workpiece reaches 600 °C with no signs of material melting. Different material flow patterns were observed in the formed tube during deformation. The material in the central region of the cylindrical workpiece moves in a spiral motion with significant rotation while the material near the outer surface of the workpiece moves in a linear path.

Keywords: Friction Stir Back Extrusion, Johnson-Cook model, severe plastic deformation, numerical modeling, Coupled Eulerian-Lagrangian modeling.

Table of Contents

List of Figures

List of Tables

Chapter 1. Introduction

1.1. Overview

The invention of friction stir welding (FSW) in 1991 paved the way for solid state manufacturing technologies to be utilized in various industrial applications. In FSW, a non-consumable rotating tool, with a specially designed pin and shoulder, is plunged at the beginning of the joint until it reaches the appropriate depth and subsequently travels over the joint line while rotating as shown in Figure 1.1. The severe plastic deformation produces fine grain microstructure at the welding zone, which leads to superior mechanical properties, fatigue properties, improved formability, and extraordinary ductility[1-3]. Recently, several derivatives of FSW have emerged taking advantage of the fine grain microstructure and the absence of an external heating source as heat is generated due to friction and plastic deformation. Friction stir spot welding, friction stir processing, ultrasonic friction stir welding, and friction stir back extrusion are examples of FSW derivatives[4-7].

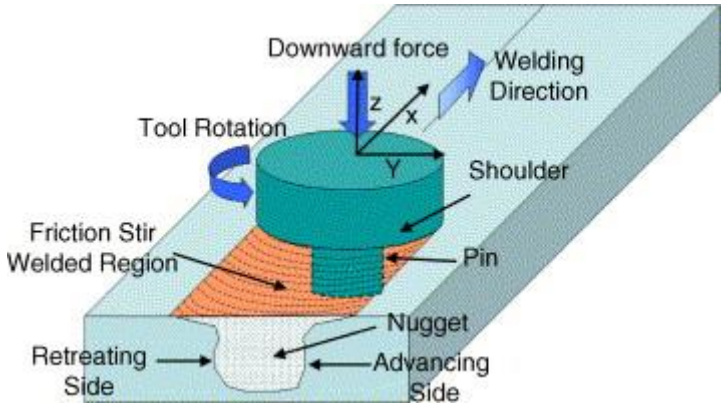

Figure 1.1: Schematic drawing of friction stir welding [8].

Friction Stir Back Extrusion (FSBE) is a new bulk deformation manufacturing process developed in the year 2012 [9]. In this process, severe plastic deformation forces the processed material to follow a three-dimensional spiral motion path inside a die using a stirring tool to produce a tube as shown in Figure 1.2. FSBE is capable of producing fine grained lightweight seamless tubes that can be used in load bearing applications. Tubular shapes have several applications in the aerospace, automotive and building industries. For example, tubular seamless lightweight sections are replacing

stamped components in the automotive industry to reduce fuel consumption and CO_2 emissions. Engine cradles, truck frames and roof rails are examples of these tubular structures. One of the main advantages of FSBE, when compared to conventional extrusion, is the absence of an external heating system. For example, in order to extrude Mg AZ31 tubes by conventional extrusion, the billet should be preheated to temperatures in excess of 300 °C. In addition, FSBE does not generate harmful fumes and produce tubes with equiaxed fine grains. As per the sustainability assessment framework proposed by Saad et al. [10], FSBE is considered a sustainable manufacturing process.

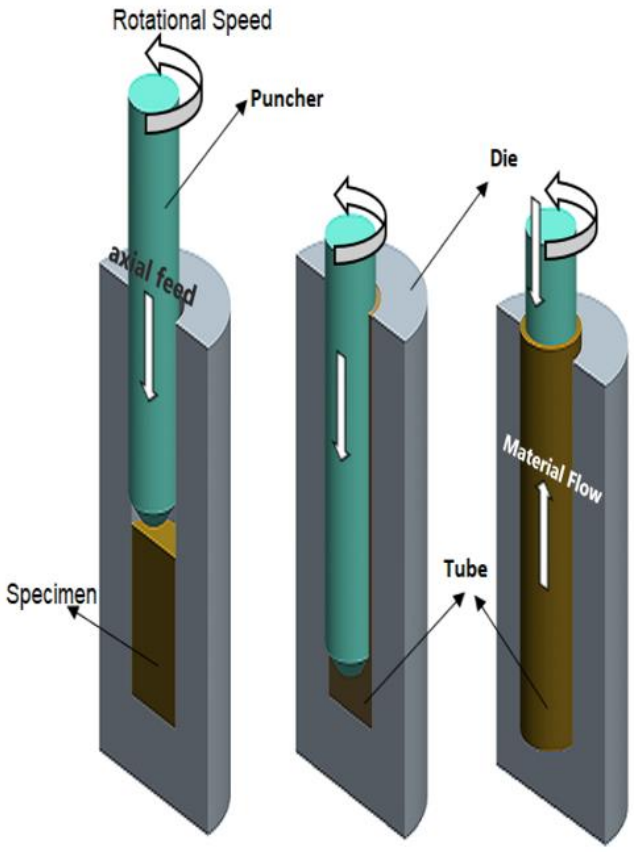

Figure 1.2: Schematic diagram of (FSBE), the figure shows the configuration of the process to produce a tube via (FSBE).

Due to the advancement in high performance computing algorithms, numerical simulations have been used extensively for modeling processes that involve severe plastic deformation and high strains in an effort to understand the material flow and the effects of process parameters on the different aspects of these processes [11-23].

Numerical modeling is a valuable tool that proved to be cost effective and accurate to model friction stir welding, friction stir spot welding, and friction stir processing. The numerical models for friction stir technologies are mainly based on the finite element and finite difference methods[24].

In the finite difference method, the integration domain (mesh/grid) is defined in a fixed Eulerian reference system and the nodes are defined as spatial points in space. This approach was used by several researchers [12, 25-27] in which the deformed material is modeled as an incompressible highly viscous non-Newtonian fluid that moves within the fixed mesh. Sticking, sliding, and partial sticking/sliding contact conditions are pre-assumed between the tool and workpiece, because the position of the moving material interfaces, are extremely difficult to determine in the Eulerian domain. Therefore, a realistic friction model such as the Columb or Tresca friction models cannot be implemented in the pure Eulerian approach. It is also very difficult to track the time history of a field variable at a specific point on the material because the movement of the material cannot be tracked using a fixed mesh. However, the main advantage of the Eulerian approach is its capability of modeling large deformation problems since material flow does not cause any mesh distortion and hence do not cause any numerical problems.

In the finite element method, a Lagrangian domain is used where mesh/grid is attached to the material throughout the computational process. A number of studies [28-35] have been performed to model the FSW using the pure Lagrangian approach. In this approach, each node in the grid follows the associated material particle and as the grid deforms, the mesh deforms accordingly. Therefore, the time history of a field variable throughout the simulation can be easily obtained. Physical based contact models that describe the contact conditions at the tool material interface can be implemented. The boundary conditions are automatically imposed because traceable grid nodes can be placed on the boundaries and material interfaces. Due to these advantages, the finite element is predominantly used in the field of solid mechanics. However, for processes that include severe plastic deformation, the excessive mesh distortion leads to highly inaccurate numerical results. To overcome the disadvantages of the pure Lagrangian description, the Arbitrary Lagrangian Eulerian (ALE) finite element method was used to simulate friction stir based processes [36-40]. In the ALE

method, Lagrangian motion is computed at the beginning of each analysis time step, then the mesh/grid can move arbitrarily in a rezoning step to optimize the shape of the elements. However, several researchers faced convergence issues in which the ALE FE model fails to converge due to the excessive deformation during friction stirring[41, 42].

The Coupled Eulerian Lagrangian (CEL) method that assigns Lagrangian and Eulerian domains separately to different regions has been recently used to simulate FSW[43-47]. The regions interact continuously through a coupling module to exchange computational information between them. In FSW, the tool is modeled using a Lagrangian domain while the welded sheets or plates are modeled using an Eulerian domain. Physical based contact models at the tool material interface can be implemented. The CEL method is capable of modeling the large deformation in the workpiece since material flow does not cause any mesh distortion and hence do not cause any numerical problems and the mechanical boundary conditions at the interface can be implemented using a physical based friction model.

1.2. Problem Statement

The physics of the FSBE is not well understood yet. FSBE is a complex process that includes highly coupled phenomena that include severe plastic deformation, heat generation due to friction and plastic deformation, tool-workpiece and die-workpiece mechanical and thermal interaction. A limited number of papers on FSBE are available in literature [7, 9, 48, 49]. The available papers focus mainly on the mechanical properties and grain structure of the produced tubes. None of these studies provide information on the material flow, strains, strains rates, or temperature history in the produced tube during deformation.

1.3. Research Significance

Climate change is becoming a major concern for humankind. According to NASA [50], the carbon dioxide levels in the air are at their highest in 650,000 years at 402.56 part per million. This created pressure on the manufacturing industry to reduce CO_2 emissions by improving the existing manufacturing processes or looking for new environmentally friendly manufacturing. Thus, FSBE is one among the manufacturing processes that have a promising future as it is an energy efficient process.

The utilization of FSBE to produce lightweight tubes with superior mechanical properties and the usage of these tubes in several applications will contribute to the reduction of CO_2 emissions. This research has a positive impact on environmental sustainability that is becoming a high priority for organizations on the local, Gulf Cooperation Council countries, and international levels.

1.4 Thesis Contribution

Previous researches have demonstrated the grain size refinement of the base material as a result of the friction stir back extrusion process. Moreover, a comparison of the mechanical properties between the FSBE processed tube and conventional manufactured tube was investigated [7, 9, 48, 49]. The present work is designed to be the first to use the finite element method to simulate the FSBE process in order to gain a deep understanding of FSBE in terms of:

- Understanding the material flow pattern and trace the material deformation path during processing.
- Investigating the strain rate distribution in the processed tubes, which cannot be measured experimentally.
- Studying the temperature profile through the processed tube wall in order to capture melting under specific process parameters.

1.5. Objectives

The main objective of this work is to gain a deep understanding of the FSBE process through numerical modeling. A Multiphysics CEL model that accounts for large plastic deformation, heat generation due to friction and plastic deformation, tool-workpiece and die-workpiece mechanical and thermal interaction is developed to simulate the FSBE process. The numerical model and experimental setup are presented first. FSBE experiments are conducted to produce Mg AZ31 seamless tubes and validate the model against experiments. After the model is validated, the numerically computed material flow pattern, strain and strain rate fields, and grain size are investigated.

Chapter 2. Finite Element Model

In FSBE, the workpiece exhibits large distortion and continuous contact with the die and the stirring tool. Pure Lagrangian representation of the workpiece might lead to inaccurate results or lack of convergence due to the severe distortion of the mesh. To overcome this problem, the workpiece is modeled as an Eulerian material that is tracked as it flows through a nondeformable mesh by computing its Eulerian volume fraction. The Eulerian volume fraction is one if the Eulerian element is completely filled. The Eulerian volume fraction is zero if the no material is in the element. The software ABAQUS will be used to model the FSBE process.

The stirring tool and the die are modeled as rigid Lagrangian bodies. The Lagrangian bodies can move through the Eulerian mesh without any thermal or frictional interaction until they encounter an Eulerian element filled with material (Eulerian volume fraction greater than zero).

2.1. Model Description

A localized tridimensional coupled Eulerian Lagrangian finite element model was developed and solved using Abaqus explicit to simulate the material flow for friction stir back extrusion under specific conditions in addition to the puncher reaction forces, temperature and the state of material processed during and after extrusion.

The model was created using Abaqus Explicit software with specific dimensions in order to match the experimental setup dimensions, the die and the puncher dimensions are illustrated in Figure 2.1. The base specimen had been designed with a 19 mm and 50 mm diameter and length respectively.

From a general point of view, the specimen is modeled as an Eulerian mesh representing the volume where the Eulerian material flows and interacts with Lagrangian parts, which are the die and the puncher. At the beginning of the CEL simulation, a portion of the Eulerian mesh is usually filled with the desired material, while the rest are considered as a void as shown in Figure 2.2. During FSBE processing, where the material starts to flow up, the Eulerian volume fraction (EVF) is calculated for each element, which represents the ratio of the material inside an element to the volume of it. Which means if the EVF is 1 then the element is completely filled with

the material, on the other hand, if EVF is 0 then the element is empty from the material or it's a void[51].

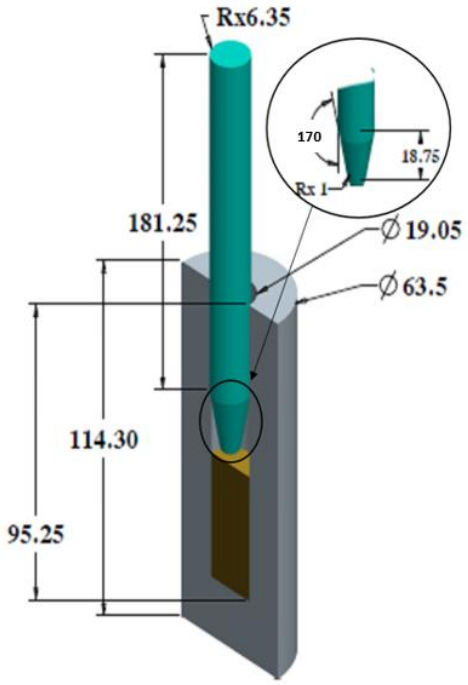

Figure 2.1: Die and Puncher dimensions (mm).

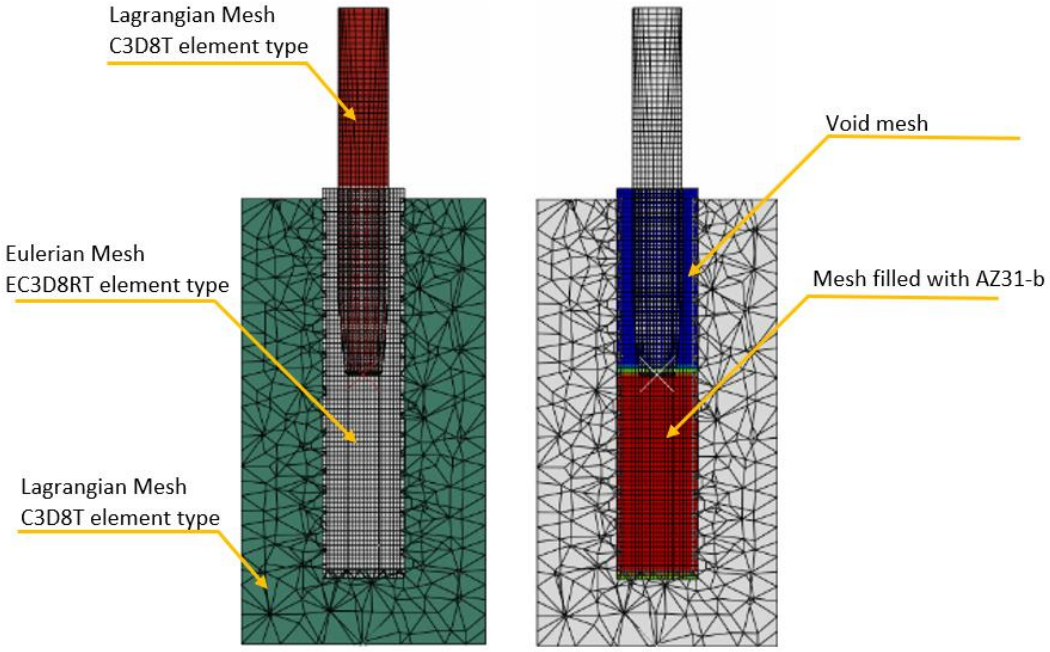

Figure 2.2: FSBE model mesh.

The model was created with 50648 nodes and 51435 elements. The die and the puncher were assigned to C3D8T trilinear displacement and temperature element type, with 1390 nodes and 6375 elements for the die and 2050 nodes and 1568 elements for the puncher. Moreover, the Eulerian part was created to be larger than the specimen dimensions in order to capture the material flow and to ensure that the material is always in the Eulerian part. for that, 21 mm diameter and 120 mm length are the dimensions of the Eulerian part while the final tube dimensions are 19 mm and 80 mm diameter and length respectively, the Eulerian part was assigned to EC3D8RT element type, this type of Eulerian elements are useful for simulations involving material that undergoes extreme deformation, up to and including fluid flow, in addition to the ability of it in calculating the thermal behavior of the deformed material. 47208 nodes and 43492 elements were assigned to the Eulerian part.

Moreover, since the FSBE process is an internal heat generated process, where the tube can be formed without an external heat source, due to friction between process parts and material deformation. Generated Heat can be computed by the equilibrium equation [24].

$$Q = P_f + r^{pL} \tag{1}$$

where Q is the heat generated per unit time per unit volume, P_f is the rate of frictional energy dissipation in the peer surfaces and r^{pL} is the rate of heat flux that is added to the model caused by plastic energy dissipated. Where $P_f \; and \; r^{pL}$ can be computed by Equation (2 and 3)

$$p_f = \tau\dot{\gamma} \tag{2}$$

$$r^{pL} = \eta\sigma_{ij}\dot{\varepsilon}_{ij}^{pl} \tag{3}$$

where η is the inelastic heat fraction, σ_{ij} is the stress tensor and $\dot{\varepsilon}_{ij}^{pl}$ is the plastic strain rate tensor, in Equation (2) $\dot{\gamma}$ is the slip rate, τ is the frictional stress, which computed by classical Coulomb's friction model Equation (4). Where τ_{Crit} is the maximum allowable friction (shear) stress across the contacted surfaces, p is contact pressure and μ friction coefficient.

$$\tau_{Crit} = \mu p \tag{4}$$

Finally, the generated heat due to friction and plastic deformation will be transferred internally across each process part according to Equation (5). Where C is the specific heat capacity, $\dot{T}$ is the temperature rate, T is the instantaneous temperature, λ is the thermal conductivity, Q is the heat flux and ∇ is defined as in Equation (6).

$$\rho C\dot{T} = \nabla(\lambda \nabla T) + Q \tag{5}$$

$$\nabla = \frac{\partial}{\partial x} + \frac{\partial}{\partial y} + \frac{\partial}{\partial z} \tag{6}$$

2.2. Material Model

Constitutive models describe the material responses to different mechanical and/or thermal loading conditions, which provide the stress–strain relations to formulate the governing equations, together with the conservation laws and kinematic relations[52].

In numerical models, the implementation of a constitutive model includes the integration of the state of the material at an integration point over a time increment during a nonlinear analysis. The implementation of constitutive models in ABAQUS assumes that the material behavior is entirely defined by local effects, so each spatial integration point can be treated independently. The mechanical constitutive models that are provided in ABAQUS often consider elastic and plastic response. In the inelastic response models that are provided in ABAQUS, the elastic and inelastic responses are distinguished by separating the deformation into recoverable (elastic) and nonrecoverable (inelastic) parts. This separation is based on the assumption that there is an additive relationship between strain rates[53]:

$$\dot{\varepsilon} = \dot{\varepsilon}_{plastic} + \dot{\varepsilon}_{elastic} \tag{7}$$

And since the FSBE is a multi-physics process where the flow stress is a function of strain, strain rate and temperature. Therefore, the behavior of Mg AZ31 is described by Johnson-Cook constitutive model. J-C model is widely used in describing the material behavior when a large strain rate takes a place [44, 45, 54]. J-C constitutive model is expressed as:

$$\sigma = (A + B\varepsilon^n)\left[1 + C\ln\frac{\dot{\varepsilon}}{\dot{\varepsilon}_0}\right](1 - (T^*)^m) \tag{8}$$

where A is the yield stress, B is the strain hardening coefficient, n is the strain hardening exponent, , m is the temperature coefficient, $\dot{\varepsilon}$ is the (plastic) strain rate, $\dot{\varepsilon}_0$ is a reference (quasi-static) strain rate and C is the strain rate sensitivity parameter[55]. For that, the first term in J-C model $(A + B\varepsilon^n)$ influences of quasi-static behavior, $\left[1 + C \ln \frac{\dot{\varepsilon}}{\dot{\varepsilon}_0}\right]$ influences of strain rate, and $\left(1 - (T^*)\right)$ influences of temperature change and their effect on the flow stress, where T^* is nondimensional temperature and it defined as:

$$T^* = \begin{cases} 0 & for \quad T < T_a \\ \dfrac{T - T_a}{T_m - T_a} & for \quad T_a \le T \le T_m \\ 1 & for \quad T_m < \mathrm{T} \end{cases}$$

where T is the instantaneous temperature and T_a is the ambient temperature. For that, when the temperature is less than the ambient temperature there will be no effect of temperature on the stress flow, however, if the temperature exceeds the material melting temperature, the material stress flow will be zero $\sigma = 0$, which means there will be no shear resistance. Table 2.1 lists the Mg AZ31 Johnson Cook parameters. The material properties of Mg AZ31 are illustrated in Table 2.2.

Table 2.1: Mg AZ31 Johnson Cook parameters[56].

A (MPa)	**B** (MPa)	**N**	**C**	**m**
172	360.73	0.45592	0.092	0.95

Table 2.2: Thermal and mechanical properties[25].

Material Property	
Density (kg/m^3)	1781
Young's Modulus (MPa)	40200
Poisson's ratio	0.34
Conductivity (J/s.m.^{o}C)	96.4
Expansion Coefficient (1/^{o}C)	2.64×10^{-5}

Inelastic Heat Fraction	0.8
Specific Heat (J/kg.^{o}C)	1050×10^{6}
Melting Temperature (^{o}C)	650
Initial Temperature (^{o}C)	25

Moreover, the die and the puncher were made of steel, the steel material properties are illustrated in Table 2.3.

Table 2.3: Thermal and mechanical properties for the steel [25, 47, 57].

Material Property	
Density (kg/m^{3})	7870
Young's Modulus (GPa)	200
Poisson's ratio	0.3
Conductivity (J/s.m.^{o}C)	55
Specific Heat (J/kg.^{o}C)	410×10^{6}

In the severe plastic deformation processes, such as the friction stir back extrusion (FSBE) process, an extremely high strain rate and temperature take a place, therefore dynamic recrystallization occurs in such processes, where dynamic recrystallization is a field of interest in metal forming processes. Since it leads to softening the grain size. The change in the grain size strongly affects material mechanical properties. Such as the yield strength and tensile strength [58-61].

Post processing analysis was done using ABAQUS to calculate the grain size of the formed tube. It is realized that the effect of increasing in strain rate during deformation is thought to have an equivalent effect to that of decreasing the temperature during deformation. This relation is characterized by Zener Holloman parameter (Z) Equation (8).

$$Z = \dot{e}\exp\left(\frac{Q}{RT}\right) \quad (9)$$

where $\dot{e}$ is the effective strain rate, T temperature, Q is activation energy of lattice diffusion, and R is the gas constant. For Magnesium AZ31b (135 kJ/mol) and (8.314472 J/K mol) for Q and R respectively[62].

Applying Zener Holloman-grain size equation for AZ31, the grain size (d) can be predicted by Equation (9) [62].

$$\ln d = 9 - 0.27 \ln Z \tag{10}$$

2.3. Boundary Conditions

Defining the boundary conditions has a strong effect on the convergence of the CEL model [12]. For that, the boundary conditions should be equivalent to the real physical conditions of the FSBE process. From a general viewpoint, the motion boundary conditions of the die were constrained to be fixed in all directions as shown in Figure 2.3, while a 2000 rpm and 90 mm/min angular velocity and feed rate respectively were assigned to the puncher. However, the boundary conditions of the Eulerian part were modeled without applying any constraints to determine the material deformation and material flow.

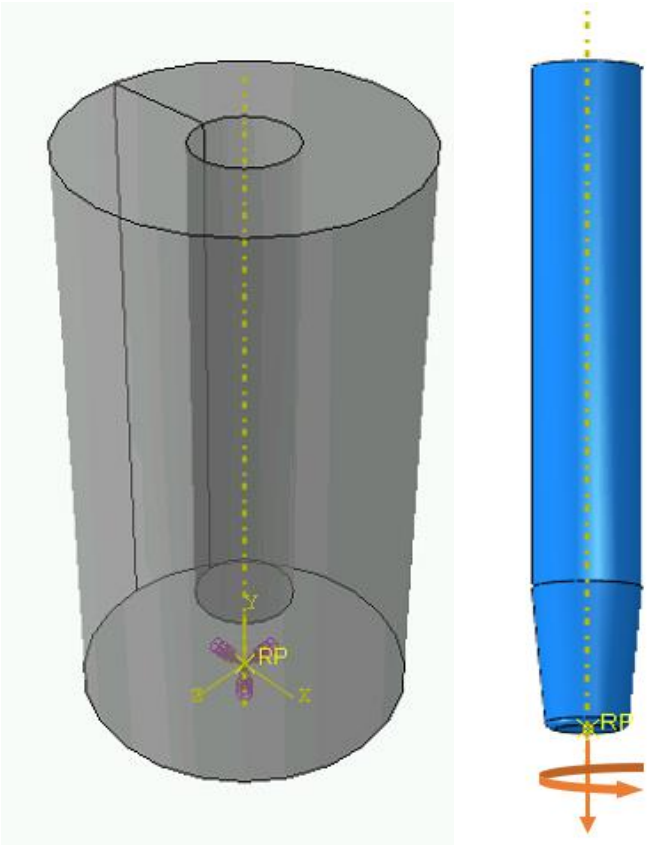

Figure 2.3: Die and puncher boundary conditions; puncher boundary conditions.

Moreover, since the thermal interaction and heat transfer through the model are important factors in simulating the FSBE process, the initial temperature was assigned through all nodes in the model to be the ambient temperature (25 ^{o}C), except the unfilled Eulerian nodes. The yellow cubes in Figure 2.4 represent the nodes constrained to the initial temperature.

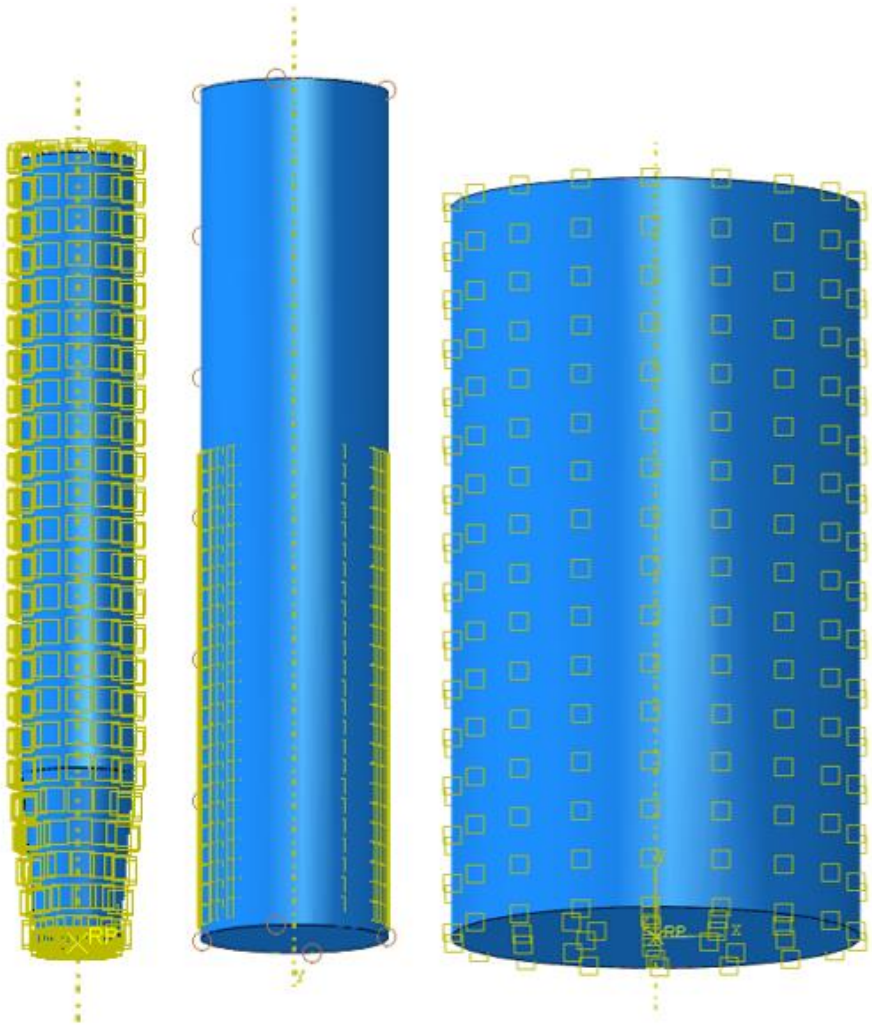

Figure 2.4: Initial temperature in Puncher, Eulerian and Die.

As mentioned before, interaction conditions and heat transfer are the most important factors in the simulation, the temperature in the FSBE process can be transferred by convection and conduction as shown in Figure 2.5. Besides the inelastic heat fraction, the contact conditions between the surfaces will affect the temperature

generation through the processing time. General contact all with self-contact domain had been used in order to simulate these phenomena. The contact conditions are illustrated in Table 2.4.

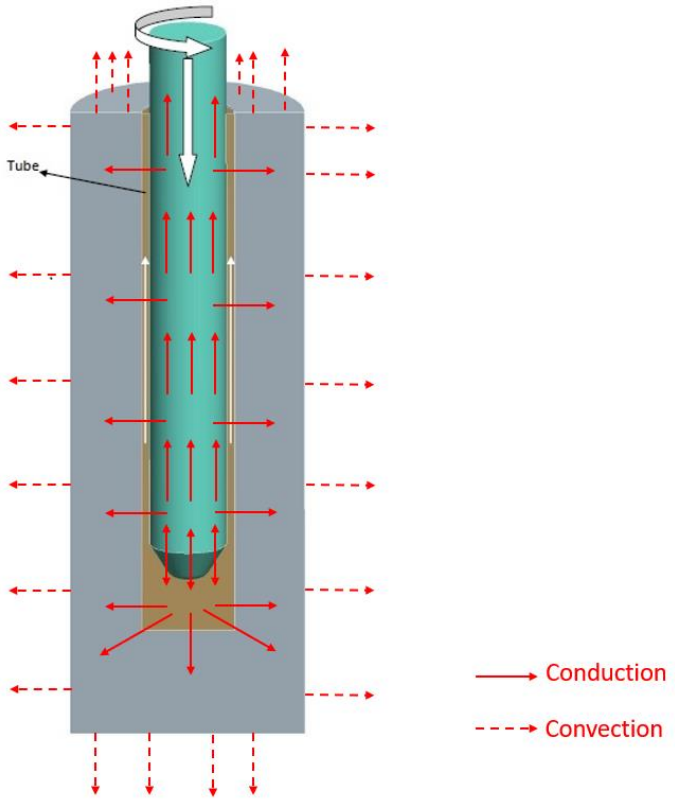

Figure 2.5: Schematic representation for the Heat flux during FSBE process.

Table 2.4: FSBE model contact conditions.

Contact condition				
Friction Coefficient				0.3
Maximum Shear Limit (MPa)				170
Thermal Conductance	Pressure (MPa)	0	1	6
	Conductance ($J/s.m^2.{}^oC$)	40×10^3	60×10^3	100×10^3
Fraction of dissipated energy caused by friction that converted to heat				1
Fraction of converted heat distributed to slave surface				0.5

2.4. Model Calibration

In order to simulate the friction stir back extrusion (FSBE) process, there are several parameters need to be calibrated. However, the complexity of the FSBE process due to the high interaction and non-linearity from mechanical and thermal aspects, make it hard to specify a certain value for these parameters. On the other hand, it is appropriate to start form friction stir welding FSW model parameters since both processes have a similar mechanical and thermal interaction properties. Figure 2.6 shows the procedure to calibrate the simulation.

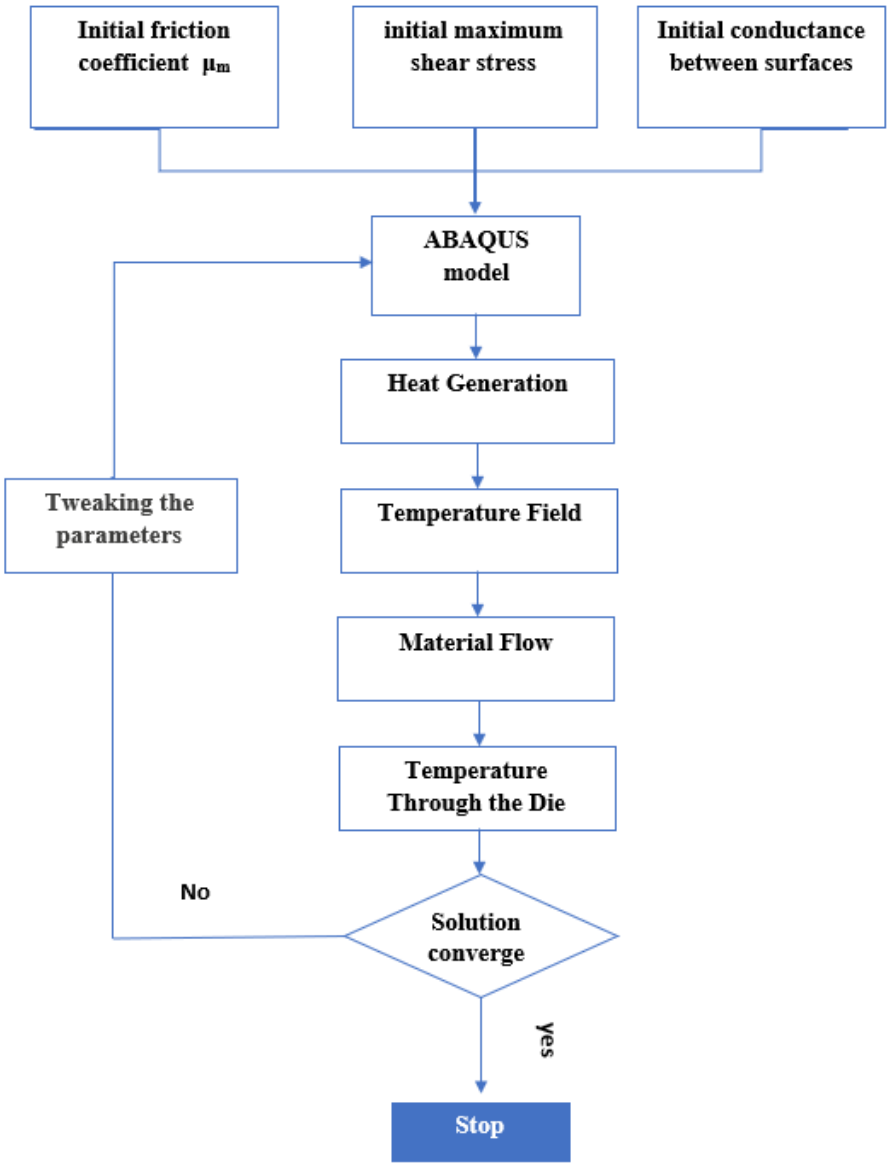

Figure 2.6: The flow chart for calibration of the FSBE Coupled Eulerian Lagrangian model.

Chapter 3. FSBE Experimental Setup and Tensile Test Procedure

3.1. FSBE Experimental Setup

Friction Stir Back Extrusion tubes were performed using DOOSAN DNM 4500 CNC turning center machine to conduct the experiments. A CAD drawing for the die is shown in Figure 3.1. The experimental setup depicted by Figure 3.2, the setup comprised of a stirring tool with a slight taper approximately (10^{o}) and a filleted head, which they lead to ease the material flow around the tool head and shoulder. In addition to the stirring tool, the extrusion die is another process component, where two pre-hardened tool steel halves assembled to form the extrusion die, caused the easiness in extracting the manufactured tubes, in order to ensure the alignment of the two halves, three cross dowel pins are used. To prevent the initial sample from rotation two screws near the bottom of the die cavity were used. Figure 3.1 illustrated the extrusion die design. While the extrusion die cavity was drilled to be 19.05 mm diameter and stirring tool with 12.7 mm diameter.

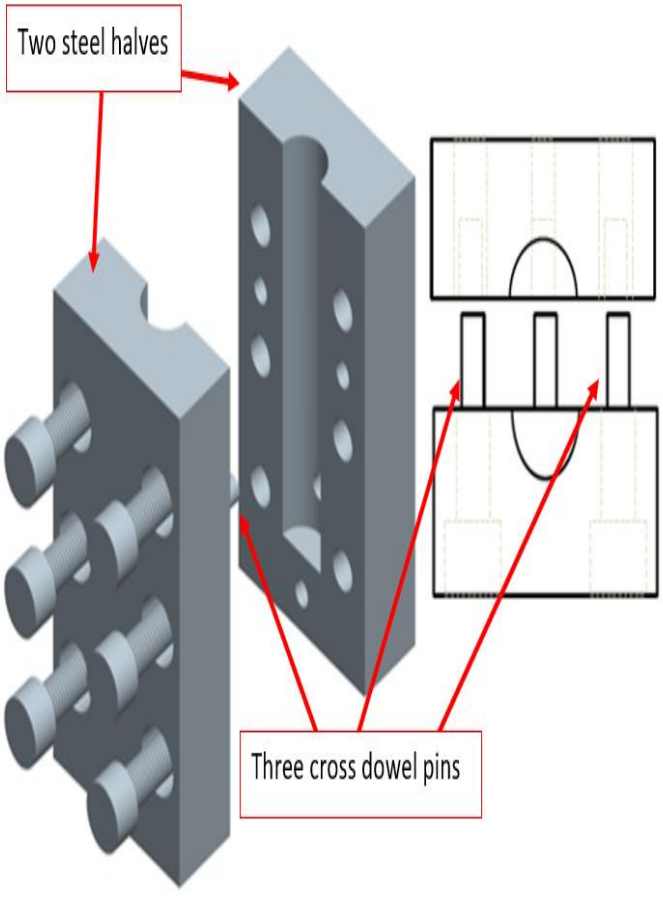

Figure 3.1: Schematic of the extrusion die.

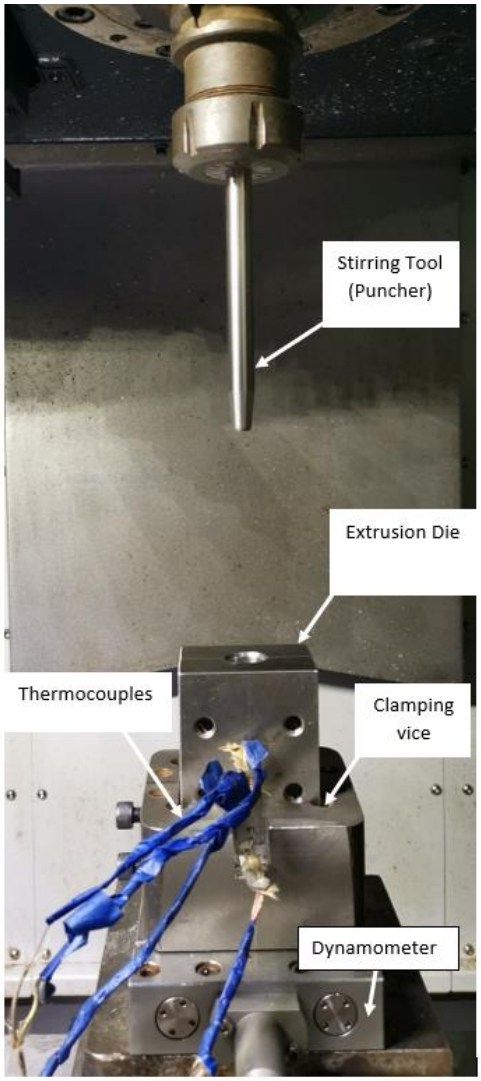

Figure 3.2: Experimental setup used to manufacture FSBE tubes.

Moreover, the die was secured to a clamping vice to avoid vibration during the FSBE process; to measure the punching force and torque Kistler 9129AA dynamometer was used and fixed at the bottom of DOOSAN DNM 4500 CNC turning center machine. The stirring tool was fitted to the machine spindle, the axisymmetric material deformation is a significant issue in the FSBE process for that the stirring tool was centered with the die cavity. Since measuring the temperature of the deformed material is impossible, several thermocouples were installed at different height into the side of the die (42 mm, 62 mm and 82 mm from the bottom of the die) in order to give a brief understanding of the heating level distribution through the material deformation during the process, also it was used to validate the finite element model.

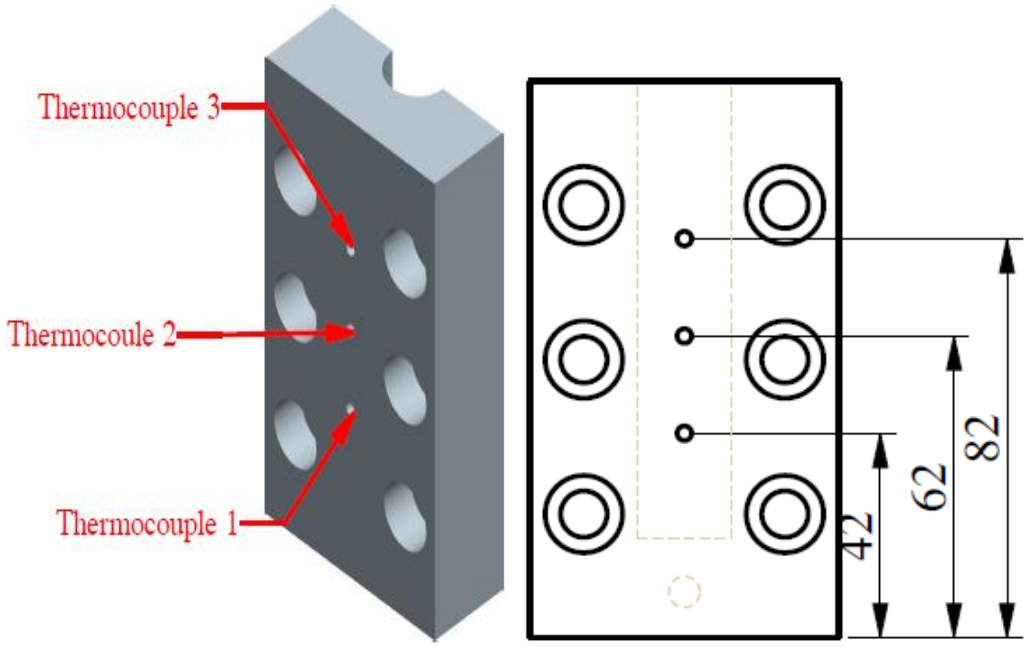

Figure 3.3: Schematic diagram of thermocouples position through the die.

3.2. FSBE Experiments Procedure

The experiments were started by preparing the AZ31-b rods that were received with 22 mm diameter and 500 mm length, CNC lathe turning center machine was used to reduce the rod diameter to 19.05 mm then 50 mm length specimens were cut to perform the starting test specimens. After that, the specimen was inserted in the extrusion die cavity. Then the stirring tool was driven, with a feed rate of 90 mm/min and a rotational speed of 2000 rpm, against the inserted specimen for 30 s to keep a 5 mm at the bottom of the generated tube as a clearance between the die and the stirring tool. Cooling the entire setup will be started once the stirring tool reaches the 5 mm clearance, to prepare for the next test. During the processing time, the punching force (Z-force) and temperature at various altitude in the extrusion die were recorded. As part of the experiment, the stirring tool was re-polished, and the die cavity was re-honed to ensure repeatability of the tube forming process.

3.3. Tensile Test Procedure

The second part of this work is studying the mechanical properties of the formed tubes, tensile specimens shown in Figure 3.4 were produced from the FSBE processed tubes using a CNC vertical milling center. The FSBE processed tubes were fabricated by the same process conditions and tube dimensions used in the CEL model. In order

to use a 3D digital Image correlation (DIC), which was used to measure the strain during the tensile test, a speckle pattern was applied to the surface of the tensile specimens. Moreover, Instron® electromechanical universal testing machine 5900 series was used to perform the tensile test of the AZ31-b samples. Figure 3.5 shows the tensile test setup with the DIC system.

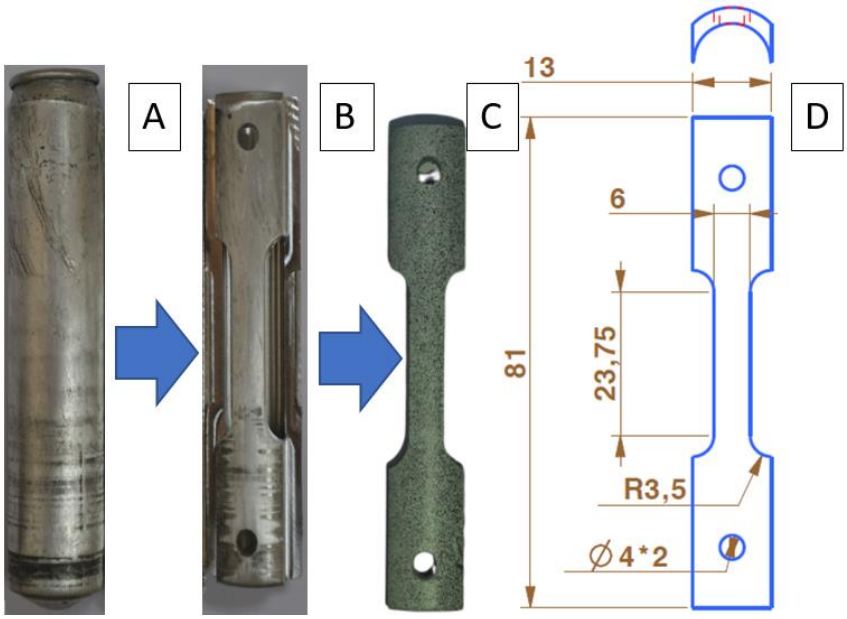

Figure 3.4: A) FSBE processed AZ31-b tube B-C) tensile sample test preparation with speckle patterns surface. D) tensile test sample dimensions.

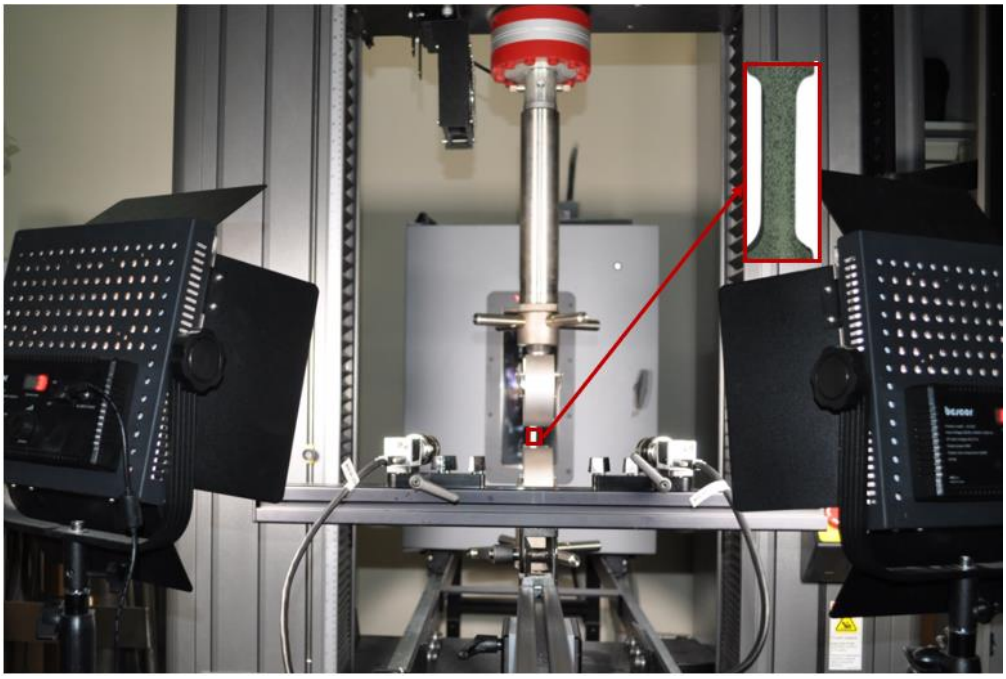

Figure 3.5: Tensile test setup using DIC system.

Chapter 4. Results and Discussion

4.1. Model Validation

In order to validate the finite element model, the experimentally recorded reactive body force in the principal loading direction (F_z) obtained from the dynamometer and the temperature recorded at three locations in the die are compared to the results obtained from the CEL model. Figure 4.1 shows that the reactive body force in the principal loading direction (F_z) obtained from experiments agrees well with the force obtained from the model. It is deduced from this figure that the force is initially high because the bar is cold. However, as heat builds up, the material softens, and the force decreases gradually due to heat accumulation. The temperature profile obtained from the thermocouples are plotted against the temperature profiles obtained from the CEL model as shown in Figure 4.2. It is clear from the figures that the temperature is higher at the initial contact region thermocouple (2), where the plastic deformation starts, due to the continuous heat accumulation in this region. It is seen from the three thermocouples readings that reasonable agreement between experiments and the CEL model is obtained.

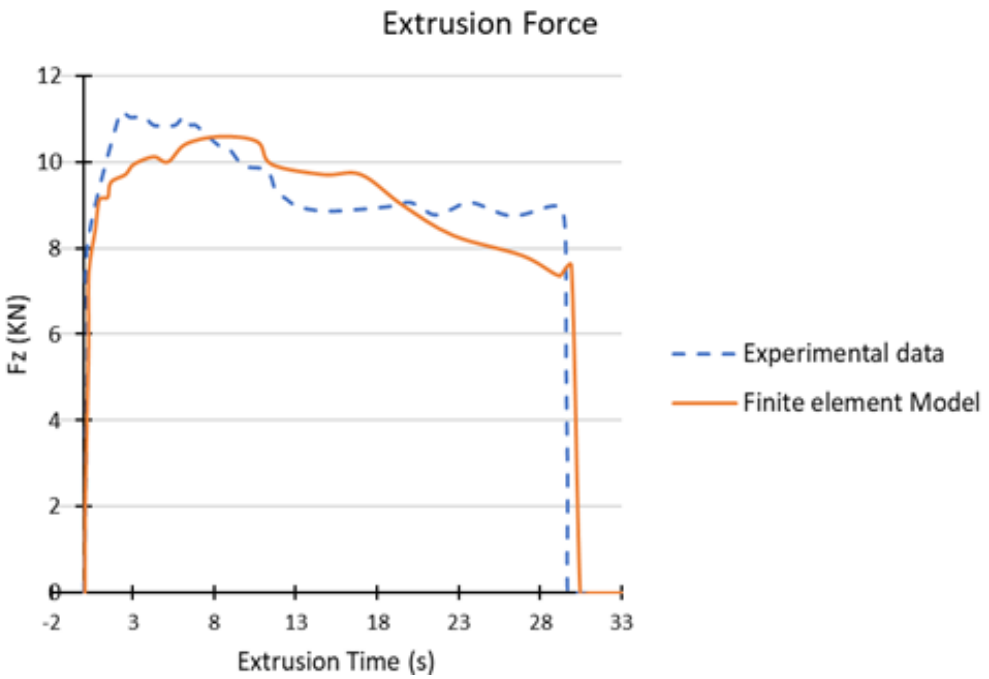

Figure 4.1: Comparison between extrusion force of experimental and Finite element data.

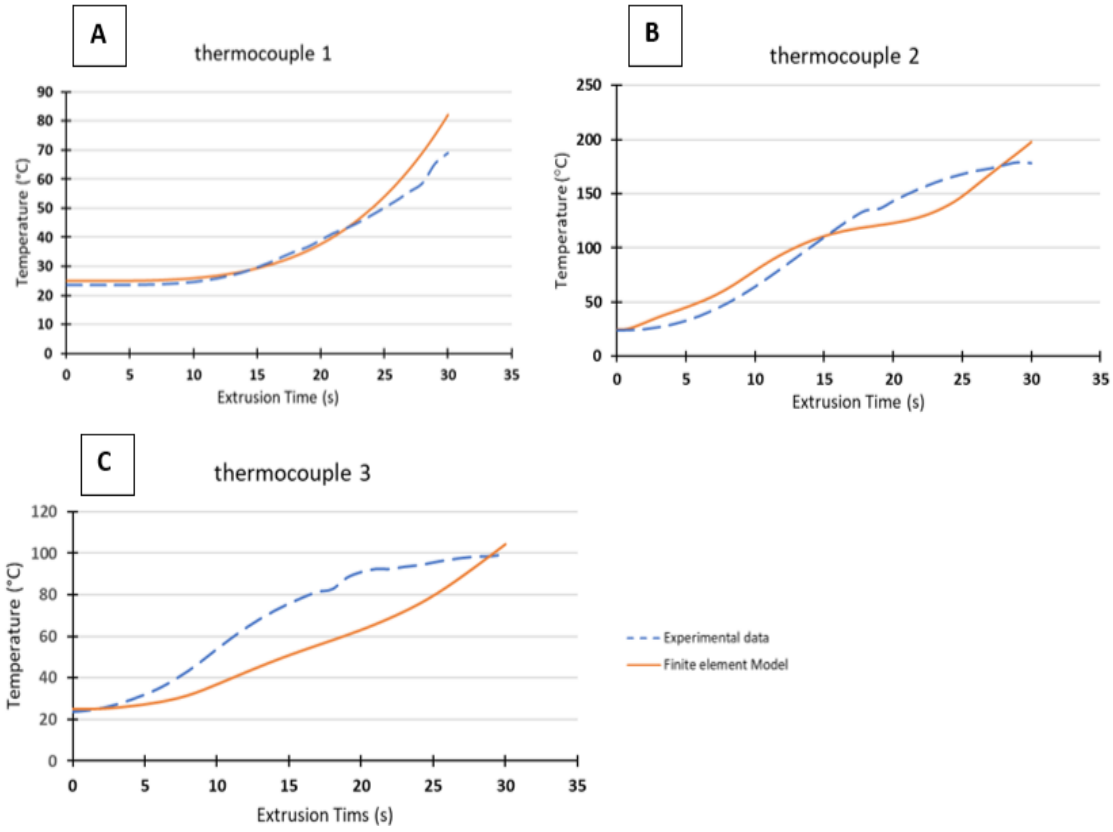

Figure 4.2: Model validation. A-C) Die temperature profile in the experiment and CEL model at different heights (Figure 3.3).

4.2. Finite Element and Experimental Results

Figure 4.3 shows the material flow pattern during the FSBE process represented by the Eulerian Volume Fraction (EVF) parameter. If an Eulerian element is empty, EVF = 0. If an Eulerian element is completely filled with material, EVF = 1. By examining the overall flow pattern during the process (Figure 4.3) and at the end of the process at different cross sections in the formed tube (Figure 4.4), it is clear that the material flow is void free (EVF = 1), uniform, and the tube has excellent structural integrity. Tensile tests for two samples were conducted to examine the integrity of the formed tube. The stress strain curves for these tests are shown in Figure 4.5. Excellent repeatability and consistency are seen from the stress strain curves. The DIC strain map is shown for several stages of deformation in Figure 4.7. It is noticed from the strain maps that the plastic deformation is highly uniform which is an indication of void free tubes. The strain is uniform up to a true strain value of 12%. Afterwards, diffuse necking starts in the tensile specimen that leads to rupture. If voids or internal defects

exist in the tube, localized strains will be present in the strain maps at an early stage of deformation and the difference between the stress strain curves for different tubes will be significant. The fractured specimens are shown in Figure 4.6.

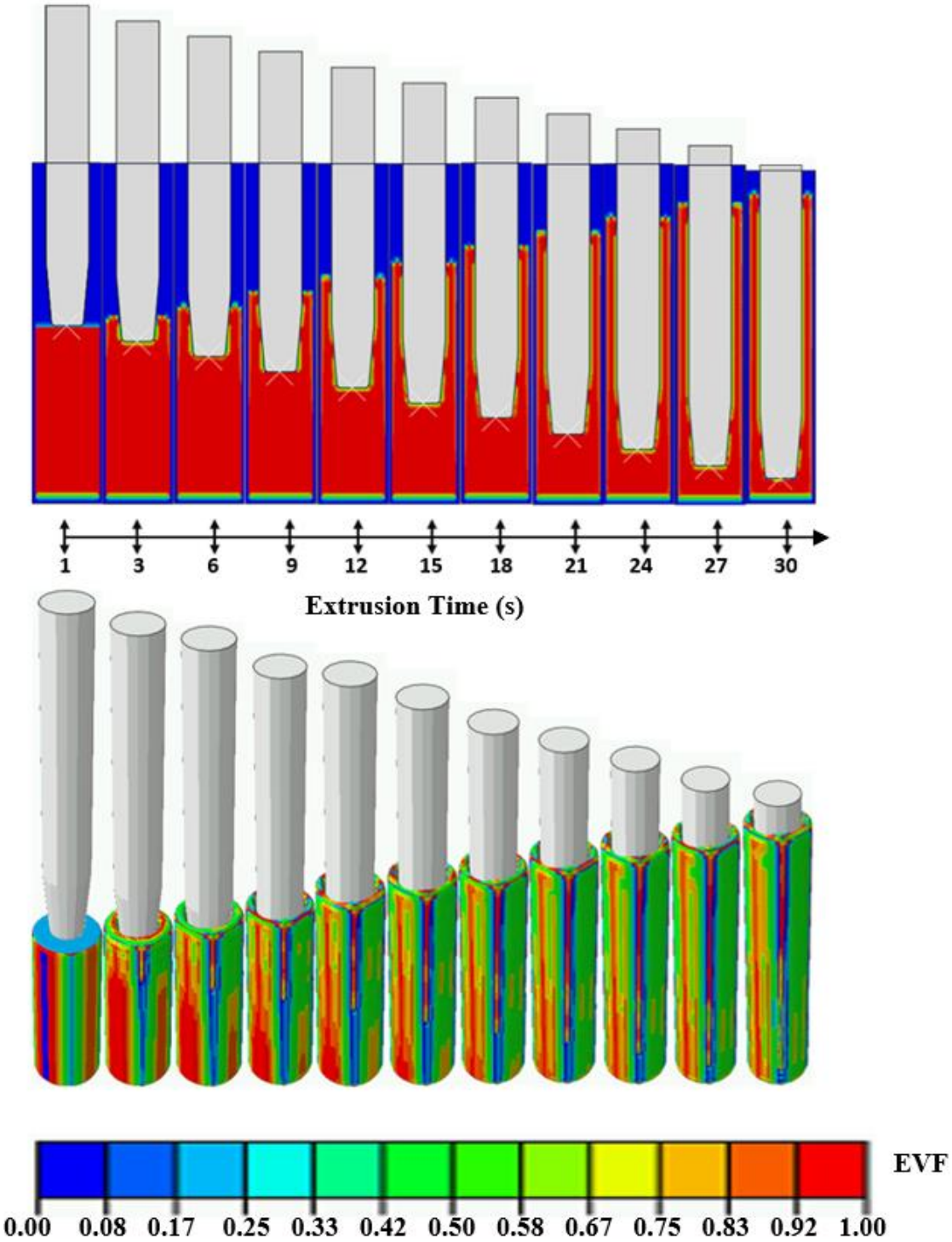

Figure 4.3: FSBE process material flow pattern.

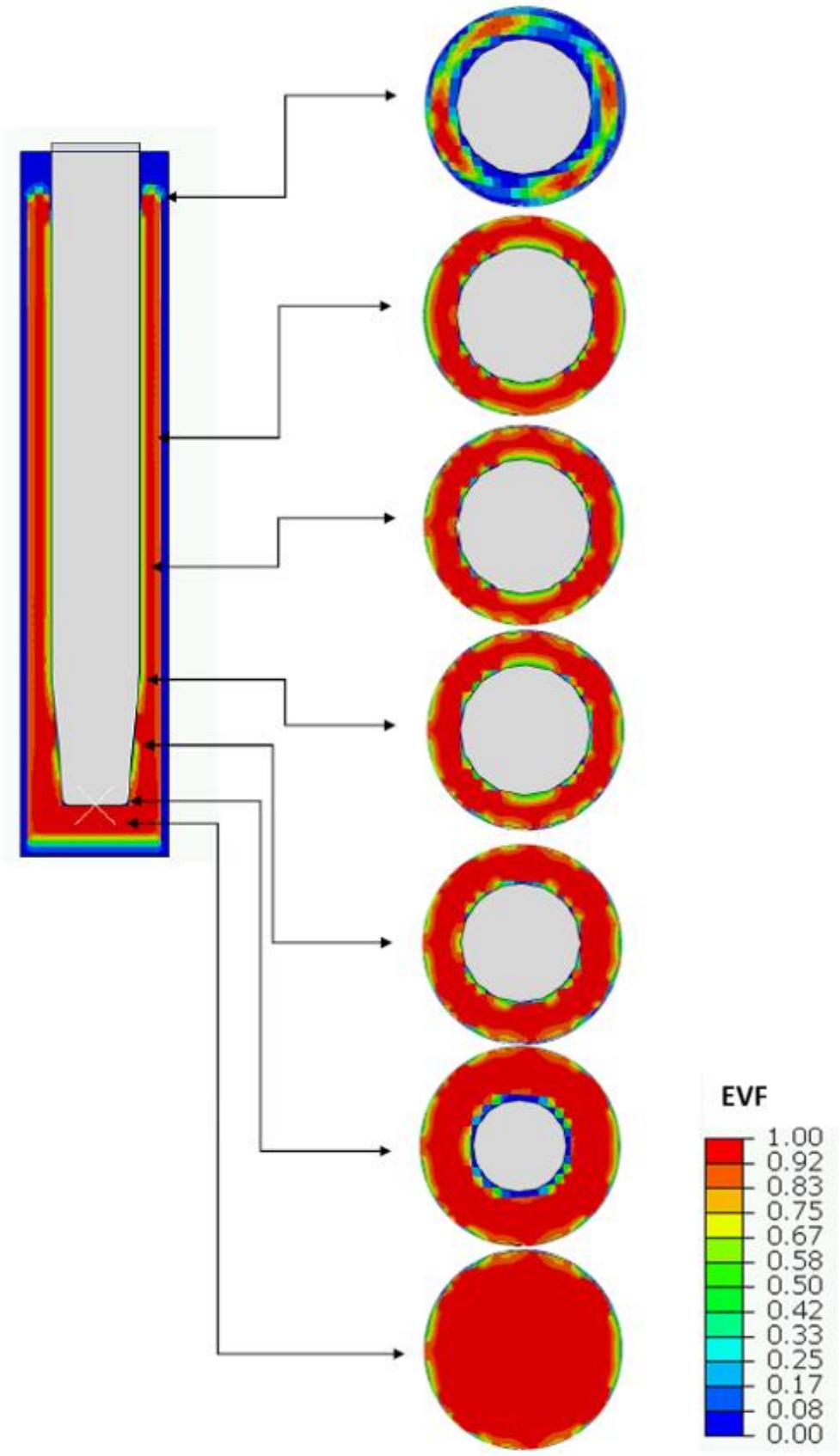

Figure 4.4: FSBE process material flow pattern for deferent cross sections at the end of the process.

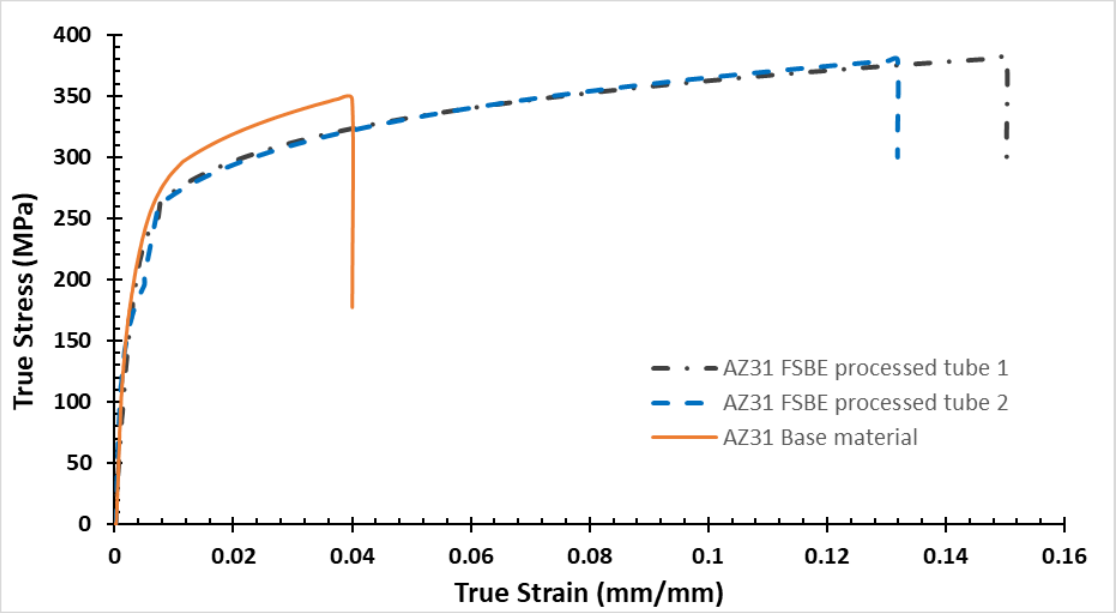

Figure 4.5: True stress strain curve of the Mg AZ31 base material tube and FSBE processed tube.

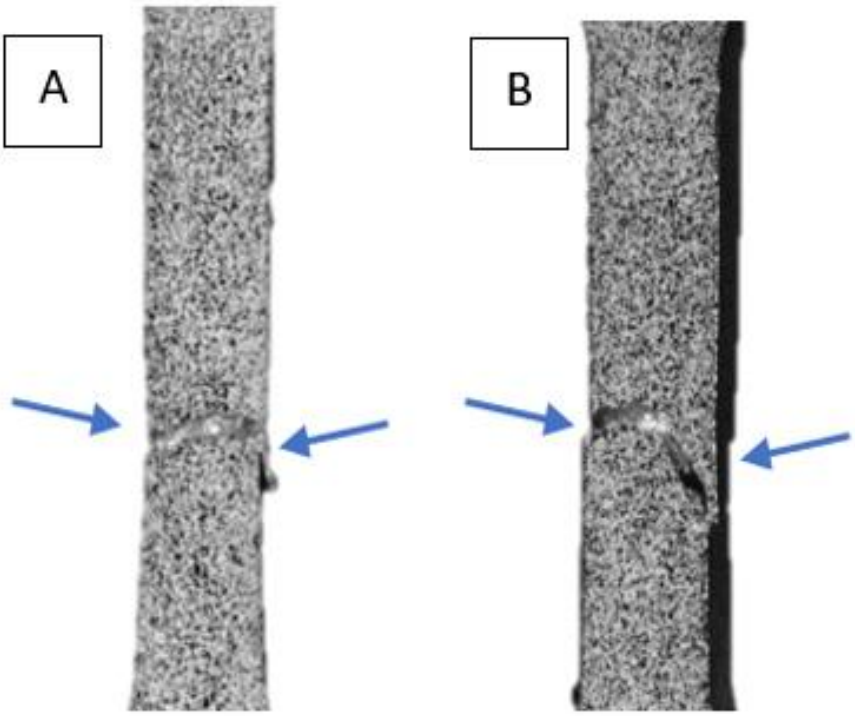

Figure 4.6: Facture of the Mg AZ31 tubes A) FSBE processed tube B) base material tube.

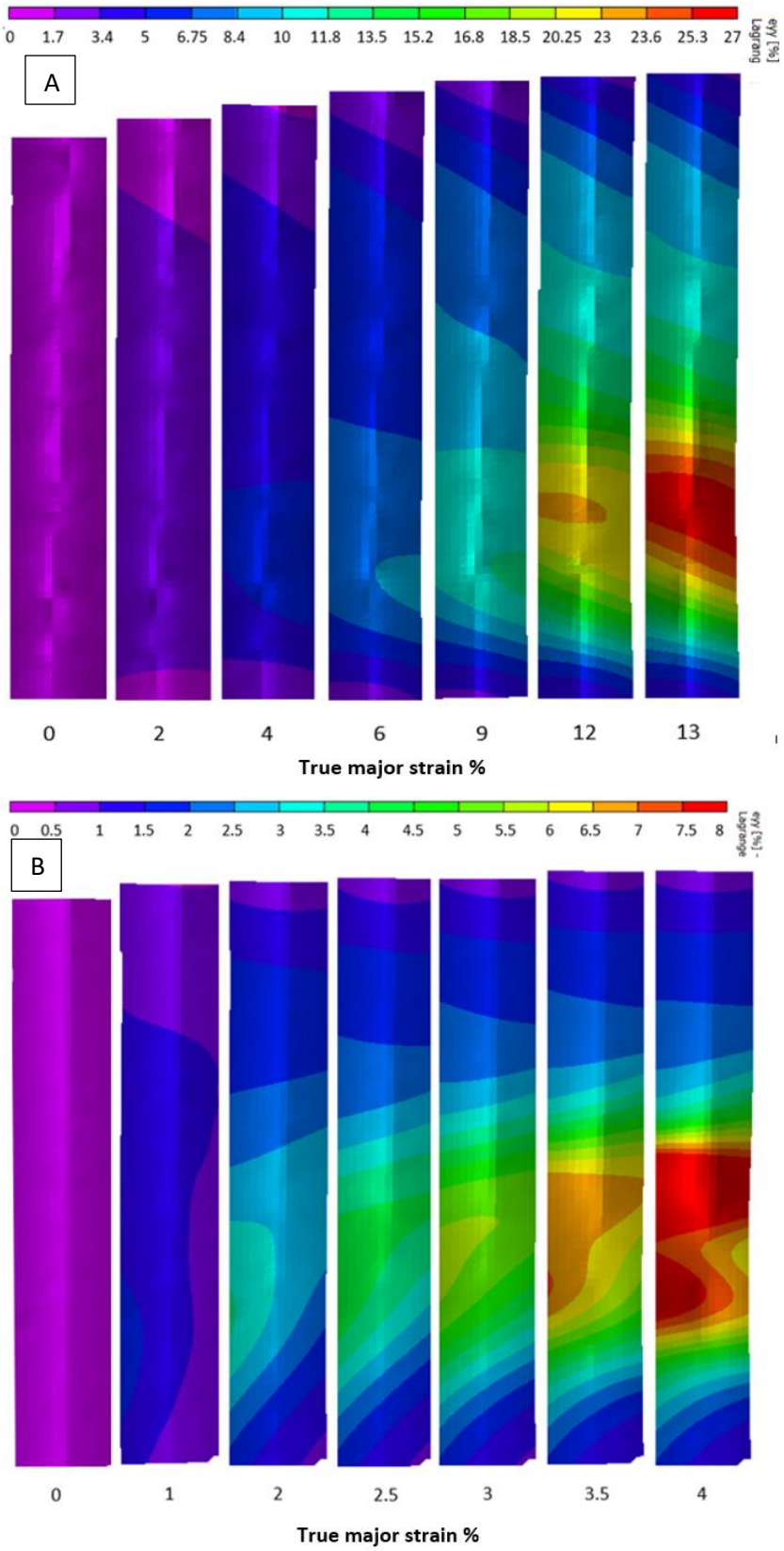

Figure 4.7: DIC plastic strain map A) for AZ31 FSBE processed tube B) for base material tube.

Figure 4.8 shows the contour plot for the temperature distribution in the formed tube at different stages of deformation, every 3 seconds starting from 0 s to 30 s. It is seen from this figure that the temperature rises initially at the tip of the tool. As the stirring tool penetrates the work piece, the temperature starts increasing at the sides of the stirring tool with a significant temperature increase observed at the tapered sides of the stirring tool. The maximum temperature in the work piece reaches 600 °C which means that material does not melt. On contrary to FSW where the temperature of the stirred zone rises then cools down due to the transverse motion of the FSW tool, continuous temperature rise is experienced in FSBE due to heat accumulation that results from the downward motion of the FSBE tool. Figure 4.9 and Figure 4.10 show a contour plot for the effective strain distribution during FSBE. The strain in the work piece is localized initially at the region adjacent to the bottom corner of the stirring tool where the material starts flowing upwards. The maximum strain is observed in the region adjacent to the tapered surface of the tool where the temperature reaches a maximum value because the material becomes softer and easier to deform.

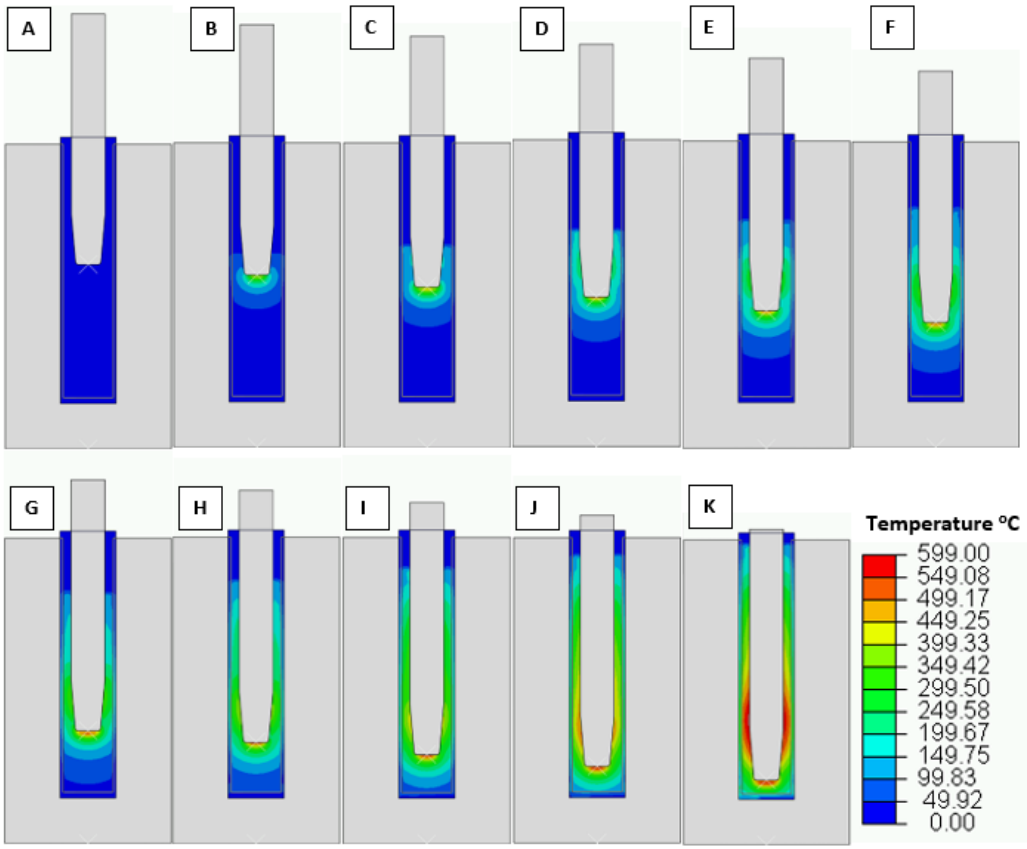

Figure 4.8: FSBE process temperature distribution.

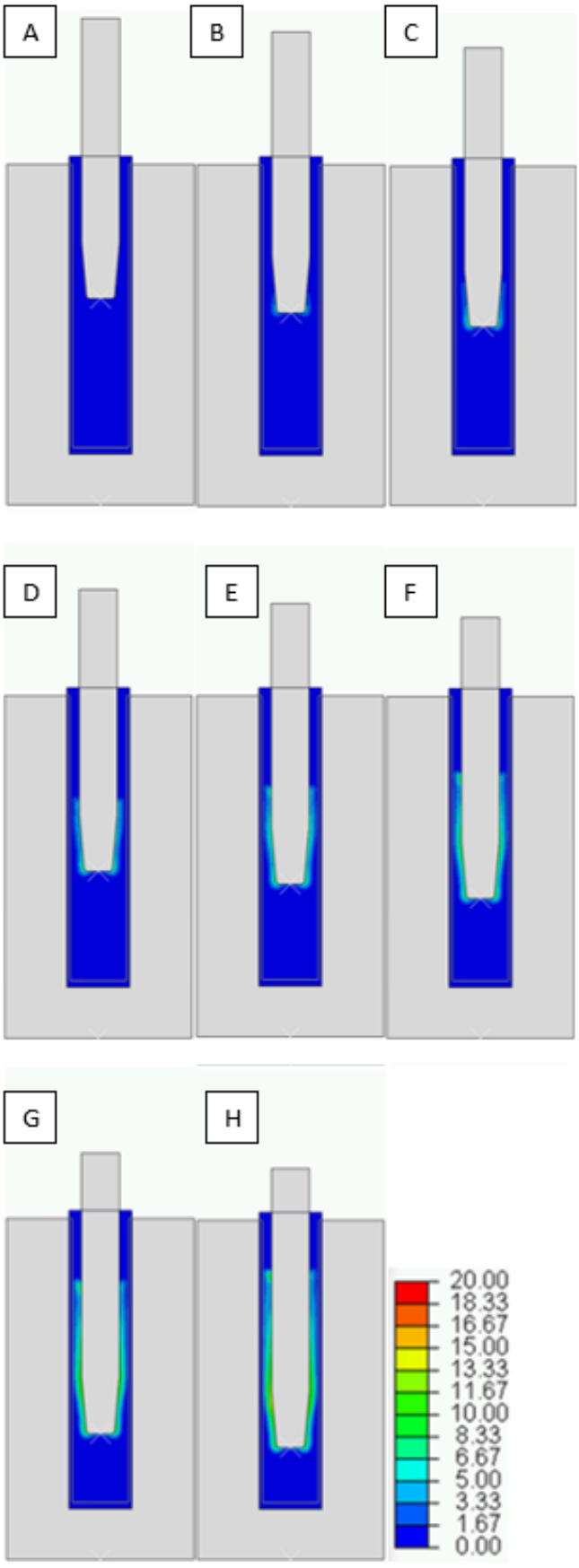

Figure 4.9: FSBE process stain distribution from 0s to 21s.

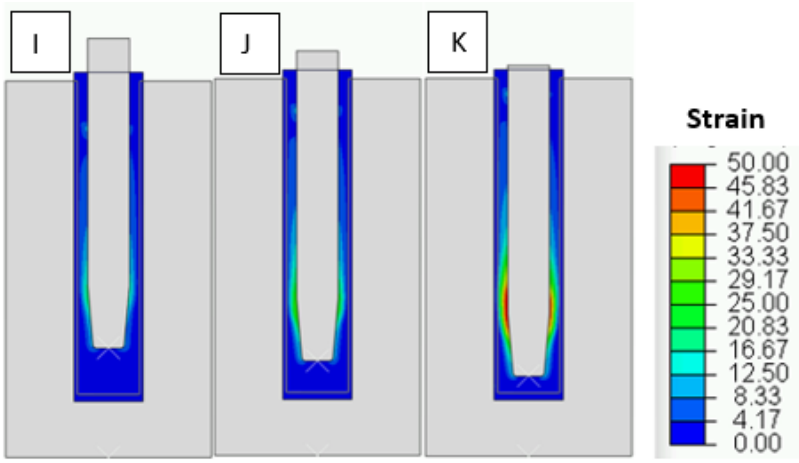

Figure 4.10: FSBE process stain distribution from 24s to 30s.

Figure 4.11 shows the strain rate distribution at different cross sections of the fully formed tube. A maximum strain rate of 70 s^{-1} is observed at the inner surface of the tube that is adjacent to the tapered region of the stirring tool. The strain rate decreases significantly through the tube thickness and reaches low values in the range of 1 s^{-1} at the outer surface of the tube. The high strain rates will lead to a series of recrystallization events known as discontinuous dynamic recrystallization (DXR). DXR will occur at the inner surface of the tube adjacent to the tapered region of the stirring tool due to the continuous straining of the workpiece material. As a result, new equiaxed fine free strain grains will be formed in this region. However, large grains the outer surface will be formed at the outer surface due to the lack shearing and severe plastic deformation. The grain size obtained from simulations is shown in Figure 4.12. The through thickness strain rate distribution and grain size results obtained here can be supported by the work done by Milner and Abu Farha [7] in which the microstructure and texture evolutions were quantified by EBSD analysis at various locations throughout the FSBE Mg AZ31 tube. In their work, the base material has an average grain size of 114 μm. The average grain size reported in the FSBE tube near the inner surface of the tube varies from 7 μm to 13 μm. However, coarse grains in the range of 80 μm were observed at the outer surface of the tube that suggest diminishing grain refinement effects as the outer surface is approached. Hence, a gradual decrease in grain size is expected as we approach the base of the tube. Milner and Abu Farha observed experimentally a gradual decrease in average grain size from 13 μm at a location near the top of the tube to 7 μm at a location close to the base of the tube.

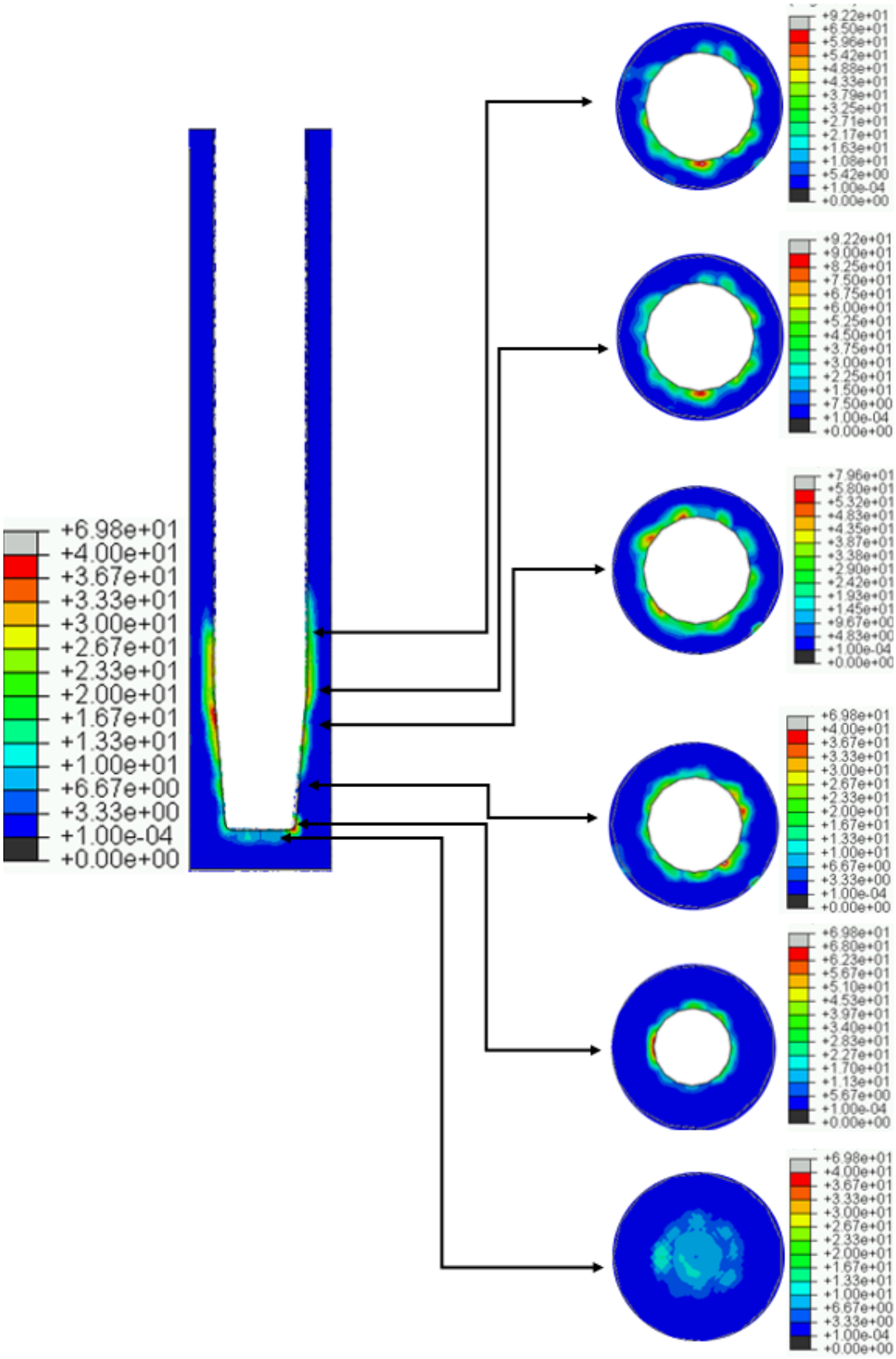

Figure 4.11: Strain rate distribution at deferent height for FSBE processed tube.

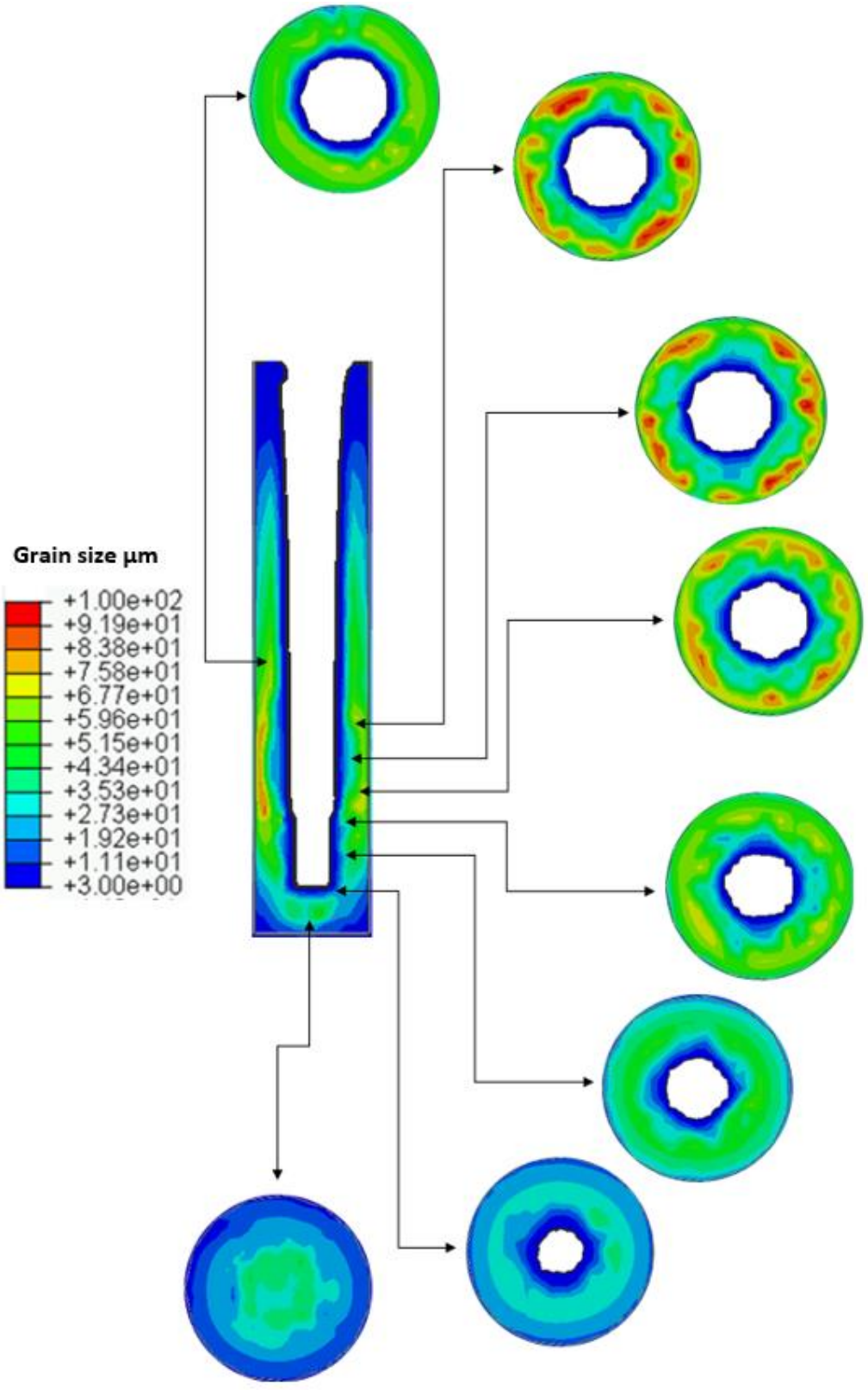

Figure 4.12: Grain size distribution for deferent cross section.

To track the material movement during deformation, tracer particles are defined at different locations in the tube. Tracer particle 1 is located at the center of the workpiece while particle 3 is located at the outer side of the tube wall, both particles are located at a height of 45 mm. Tracer particles 2,4 and 5 are at the same height 35 mm but at different radial locations. Figure 4.13 shows the position of the particles at different specimen heights.

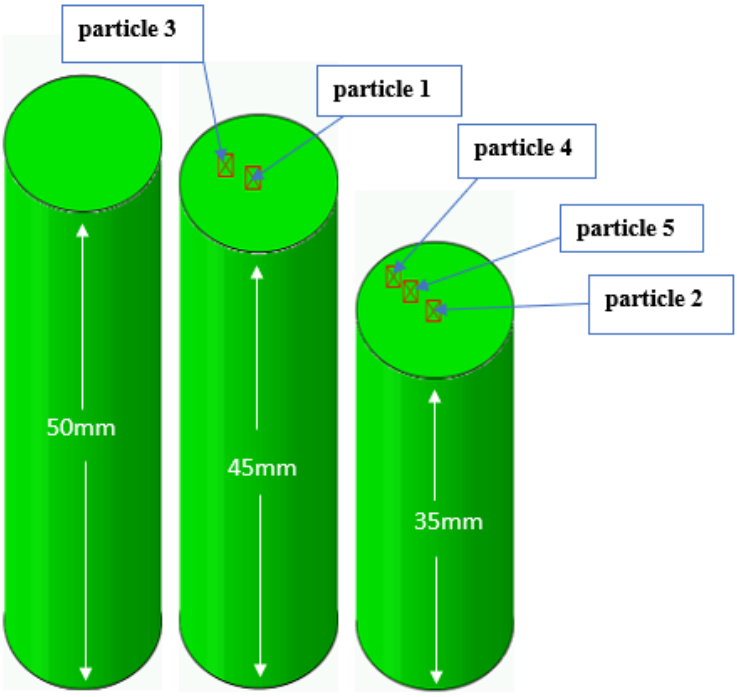

Figure 4.13: Tracer particles location in FSBE sample.

Figure 4.14 shows the path that the particles follow during deformation. It is observed from this figure that particles 1 and 2, which they are located at the center of the specimen, start their deformation with a spiral motion under the puncher tip at the beginning of the process, because of temperature increase at the sides of the puncher and the puncher rotational speed, the particles will follow the less resistive path. As a result, particles 1 and 2 will have a spiral-extrusion motion. However, particles 3,4, and 5 will have a typical extrusion material deformation that with minor influence from the tool rotational speed. As a result of that, the strain rate decreases significantly through the tube thickness.

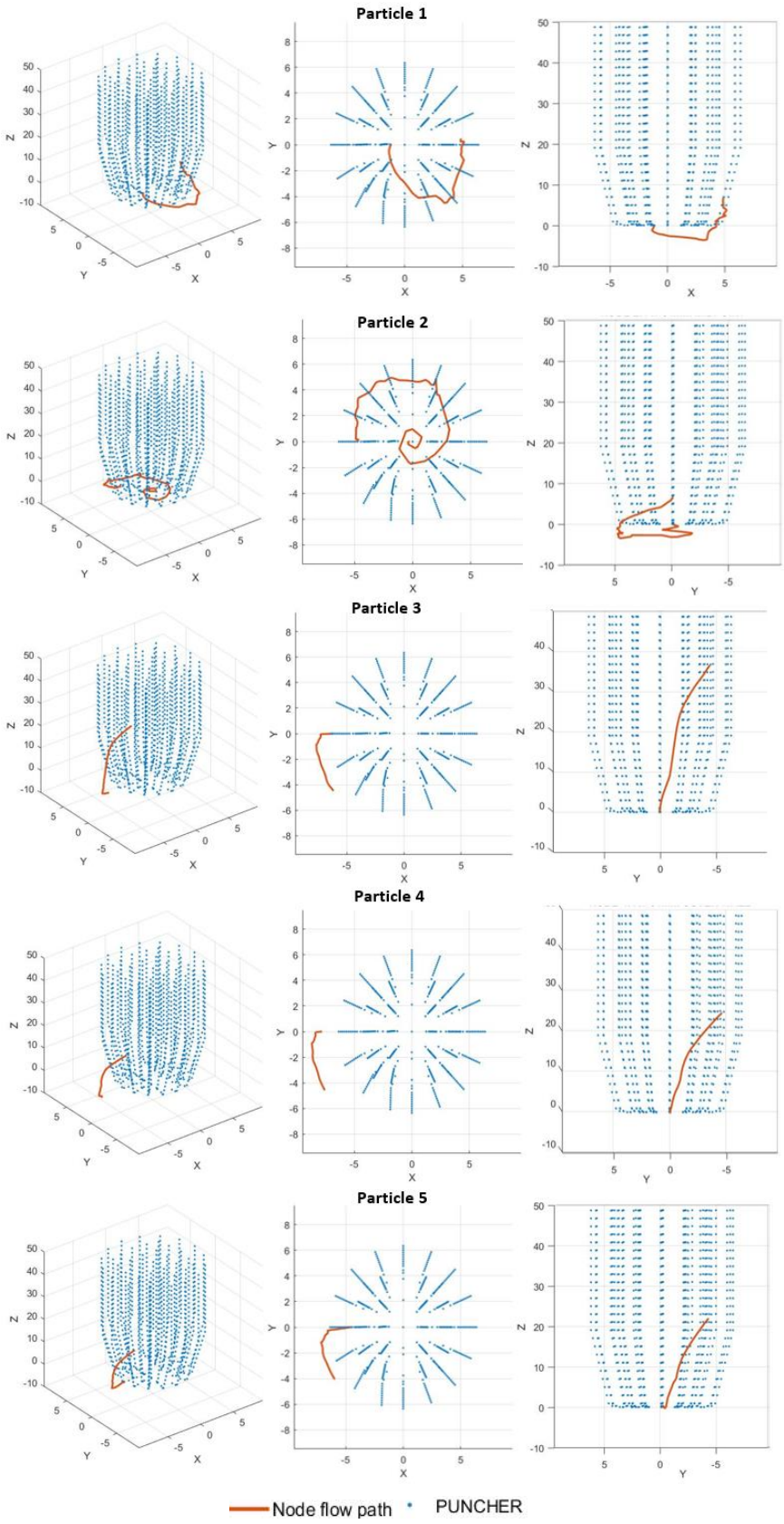

Figure 4.14: Tracer particles path at deferent location for FSBE tube all dimensions in (mm).

Figure 4.15 shows the FSBE formed tube, it is obvious from the figure that the tube outer surface has a tilted material path, and by calculating the slope of the red dashed line it was found to be tilted by an angle = 1.4^{o}, in the same way, from Figure 4.14 the tilted angle was calculated for the particles path to be equal 1.3^{o}. This can illustrate the effect of the rotational speed on the material deformation since the outer particles extrude backwardly with a slight effect of the rotational speed.

Figure 4.15: Tilted path of FSBE formed tube.

Chapter 5. Conclusion and Future Work

In this work, a Multiphysics coupled Eulerian Lagrangian model was developed using to simulate the friction stir back extrusion process. The model was validated by the calculated and the measured punching force (F_z) and die temperature profile at different heights. Therefore, the finite element simulation provides an elaborate understanding of the material flow deformation and temperature distribution through the tube processing time, which lead to explain the strain and strain rate distribution in the tube wall. And a post processing approach was done to calculate the grain size distribution using Zener Holloman equation. The main conclusions are:

- The numerical model is able to capture the reactive body force in the principal loading direction and the temperature history in the die with very good agreement with experiments.
- Void free deformation is observed by examining the material flow pattern obtained from simulations. The tensile test results and DIC maps for the tensile specimens extracted from the formed tubes support this conclusion.
- Continuous temperature rise is experienced during deformation due to heat accumulation that results from material stirring and friction as the stirring tool moves downward. The maximum temperature in the workpiece reaches 600 °C in the vicinity of the tapered sides of the stirring tool towards the end of the FSBE process.
- A maximum strain rate of 70 s^{-1} is observed at the inner surface of the tube that is adjacent to the tapered region of the stirring tool. The strain rate decreases significantly through the tube thickness and reaches low values in the range of 1 s^{-1} at the outer surface of the tube.
- The grain size was calculated at different cross section in the formed tube. Non-homogeneous through-thickness grain size was observed with significant grain refinement near the inner wall of the tube. The grain refinement diminishes as the outer wall of the tube is approached.
- Different material flow patterns were observed in the formed tube during deformation. The material in the central region of the cylindrical workpiece moves in a spiral motion with significant rotation while the material near the outer surface of the workpiece moves in a linear path.

Design of experiments can be performed as a future work by varying feed, rotational speed, and die tool clearance and study their effect on the deformation material behavior, grain size distribution, and the mechanical properties of the formed tubes. The formability of the formed tubes can also be tested by three-point bending test. Fractography analysis using confocal microscopoy and scanning electron microscope can be used to analyze the fracture behavior of the formed tube and compare it to the base material. Moreover, the effect using cooling fluid on the mechanical and thermal properties of the manufactured tubes is an important aspect that could be part of future study.

References

[1] S. Chen, X. Li, X. Jiang, T. Yuan, and Y. Hu, "The effect of microstructure on the mechanical properties of friction stir welded 5A06 Al Alloy," *Materials Science and Engineering: A*, vol. 735, pp. 382-393, 2018.

[2] P. K. Sahu and S. Pal, "Effect of FSW parameters on microstructure and mechanical properties of AM20 welds," *Materials and Manufacturing Processes*, vol. 33, no. 3, pp. 288-298, 2017.

[3] E. Cetkin, Y. H. Çelik, and S. Temiz, "Microstructure and mechanical properties of AA7075/AA5182 jointed by FSW," *Journal of Materials Processing Technology*, vol. 268, pp. 107-116, 2019.

[4] B. M. Darras, M. K. Khraisheh, F. K. Abu-Farha, and M. A. Omar, "Friction stir processing of commercial AZ31 magnesium alloy," *Journal of Materials Processing Technology*, vol. 191, no. 1-3, pp. 77-81, 2007.

[5] H. Liu, Y. Hu, S. Du, and H. Zhao, "Microstructure characterization and mechanism of acoustoplastic effect in friction stir welding assisted by ultrasonic vibrations on the bottom surface of workpieces," *Journal of Manufacturing Processes*, vol. 42, pp. 159-166, 2019.

[6] S. Suresh, K. Venkatesan, E. Natarajan, and S. Rajesh, "Influence of tool rotational speed on the properties of friction stir spot welded AA7075-T6/Al2O3 composite joint," *Materials Today: Proceedings*, 2019.

[7] J. L. Milner and F. Abu-Farha, "On the manufacture of lightweight alloy tubes via friction stir back extrusion: process evaluation and material performance," in *ASME 2014 International Manufacturing Science and Engineering Conference collocated with the JSME 2014 International Conference on Materials and Processing and the 42nd North American Manufacturing Research Conference*, 2014, vol. Volume 2: Processing, V002T02A085.

[8] R. S. Mishra and Z. Y. Ma, "Friction stir welding and processing," *Materials Science and Engineering: R: Reports*, vol. 50, no. 1-2, pp. 1-78, 2005.

[9] F. Abu-Farha, "A preliminary study on the feasibility of friction stir back extrusion," *Scripta Materialia*, vol. 66, no. 9, pp. 615-618, 2012.

[10] M. H. Saad, M. A. Nazzal, and B. M. Darras, "A general framework for sustainability assessment of manufacturing processes," *Ecological Indicators*, vol. 97, pp. 211-224, 2019.

[11] C. L. Yang, C. S. Wu, and L. Shi, "Analysis of friction reduction effect due to ultrasonic vibration exerted in friction stir welding," *Journal of Manufacturing Processes*, vol. 35, pp. 118-126, 2018.

[12] A. F. Hasan, "CFD modelling of friction stir welding (FSW) process of AZ31 magnesium alloy using volume of fluid method," *Journal of Materials Research and Technology*, vol. 8, no. 2, pp. 1819-1827, 2019.

[13] F. K. Abu-Farha, L. G. Hector, and M. A. Nazzal, "On the Development of Viable Cruciform-Shaped Specimens: Towards Accurate Elevated Temperature Biaxial Testing of Lightweight Materials," *Key Engineering Materials*, vol. 433, pp. 93-101, 2010.

[14] M. Alkhader, M. Nazzal, and K. Louca, "Design of bending dominated lattice architectures with improved stiffness using hierarchy," *Proceedings of the Institution of Mechanical Engineers, Part C: Journal of Mechanical Engineering Science*, vol. 233, no. 11, pp. 3976-3993, 2018.

[15] A. Ghandehariun, M. Nazzal, H. A. Kishawy, and U. Umer, "On modeling the deformations and tool-workpiece interactions during machining metal matrix composites," *The International Journal of Advanced Manufacturing Technology*, vol. 91, no. 5, pp. 1507-1516, 2017.

[16] F. S. Jarrar and M. A. Nazzal, "Inclination Angle Effect on the Thickness Distribution in a Superplastic Formed Long Rectangular Pan," *Materials Science Forum*, vol. 735, pp. 155-161, 2013.

[17] M. K. Khraisheh, F. K. Abu-Farha, M. A. Nazzal, and K. J. Weinmann, "Combined Mechanics-Materials Based Optimization of Superplastic Forming of Magnesium AZ31 Alloy," *CIRP Annals*, vol. 55, no. 1, pp. 233-236, 2006.

[18] M. Nazzal, F. Abu-Farha, and R. Curtis, "Finite Element Simulations for Investigating the Effects of Specimen Geometry in Superplastic Tensile Tests," *Journal of Materials Engineering and Performance*, vol. 20, no. 6, pp. 865-876, 2011.

[19] M. A. Nazzal and F. K. Abu-Farha, "Finite Element Modeling of Superplastic Forming of Tubular Shapes," *Key Engineering Materials*, vol. 433, pp. 179-184, 2010.

[20] M. A. Nazzal and A. G. Al Sabouni, "The effects of pressure control technique on hot gas blow forming of Mg AZ31 sheets," *International Journal of Material Forming*, vol. 12, no. 4, pp. 519-533, 2019.

[21] M. A. Nazzal and M. K. Khraisheh, "The Effects of Stress State and Cavitation on Deformation Stability During Superplastic Forming," *Journal of Materials Engineering and Performance*, vol. 16, no. 2, pp. 200-207, 2007.

[22] M. A. Nazzal, M. K. Khraisheh, and F. K. Abu-Farha, "The effect of strain rate sensitivity evolution on deformation stability during superplastic forming," *Journal of Materials Processing Technology*, vol. 191, no. 1, pp. 189-192, 2007.

[23] M. A. Nazzal, M. K. Khraisheh, and B. M. Darras, "Finite element modeling and optimization of superplastic forming using variable strain rate approach," *Journal of Materials Engineering and Performance*, vol. 13, no. 6, pp. 691-699, 2004.

[24] E.-z. Gao, X.-x. Zhang, C.-z. Liu, and Z.-y. Ma, "Numerical simulations on material flow behaviors in whole process of friction stir welding," *Transactions of Nonferrous Metals Society of China*, vol. 28, no. 11, pp. 2324-2334, 2018.

[25] S. Aljoaba, O. Dillon, M. Khraisheh, and I. S. Jawahir, "Modeling the Effects of Coolant Application in Friction Stir Processing on Material Microstructure Using 3D CFD Analysis," *Journal of Materials Engineering and Performance*, vol. 21, no. 7, pp. 1141-1150, 2011.

[26] M. P. Miles, T. W. Nelson, C. Gunter, F. C. Liu, L. Fourment, and T. Mathis, "Predicting recrystallized grain size in friction stir processed 304L stainless steel," *Journal of Materials Science & Technology*, vol. 35, no. 4, pp. 491-498, 2019.

[27] G. Chen, G. Wang, Q. Shi, Y. Zhao, Y. Hao, and S. Zhang, "Three-dimensional thermal-mechanical analysis of retractable pin tool friction stir welding process," *Journal of Manufacturing Processes*, vol. 41, pp. 1-9, 2019.

[28] M. Z. H. Khandkar, J. A. Khan, A. P. Reynolds, and M. A. Sutton, "Predicting residual thermal stresses in friction stir welded metals," *Journal of Materials Processing Technology*, vol. 174, no. 1, pp. 195-203, 2006.

[29] L. Fratini, G. Buffa, and R. Shivpuri, "Improving friction stir welding of blanks of different thicknesses," *Materials Science and Engineering: A,* vol. 459, no. 1, pp. 209-215, 2007.
[30] M. Khandkar, J. A. Khan, and A. P. Reynolds, "Prediction of temperature distribution and thermal history during friction stir welding: input torque based model," *Science and Technology of Welding and Joining,* vol. 8, no. 3, pp. 165-174, 2003.
[31] G. Buffa, L. Fratini, and M. Piacentini, "On the influence of tool path in friction stir spot welding of aluminum alloys," *Journal of Materials Processing Technology,* vol. 208, no. 1, pp. 309-317, 2008.
[32] C. Chen and R. Kovacevic, "Finite element modeling of friction stir welding—thermal and thermomechanical analysis," *International Journal of Machine Tools and Manufacture,* vol. 43, no. 13, pp. 1319-1326, 2003.
[33] G. Buffa, J. Hua, R. Shivpuri, and L. Fratini, "A continuum based fem model for friction stir welding—model development," *Materials Science and Engineering: A,* vol. 419, no. 1, pp. 389-396, 2006.
[34] V. Soundararajan, S. Zekovic, and R. Kovacevic, "Thermo-mechanical model with adaptive boundary conditions for friction stir welding of Al 6061," *International Journal of Machine Tools and Manufacture,* vol. 45, no. 14, pp. 1577-1587, 2005.
[35] L. Fratini, G. Buffa, D. Palmeri, J. Hua, and R. Shivpuri, "Material flow in FSW of AA7075-T6 butt joints: continuous dynamic recrystallization phenomena," *Journal of Engineering Materials and Technology,* vol. 128, no. 3, pp. 428-435, 2006.
[36] M. Assidi, L. Fourment, S. Guerdoux, and T. Nelson, "Friction model for friction stir welding process simulation: Calibrations from welding experiments," *International Journal of Machine Tools and Manufacture,* vol. 50, no. 2, pp. 143-155, 2010.
[37] K. N. Salloomi, "Fully coupled thermomechanical simulation of friction stir welding of aluminum 6061-T6 alloy T-joint," *Journal of Manufacturing Processes,* vol. 45, pp. 746-754, 2019.
[38] L. Long, G. Chen, S. Zhang, T. Liu, and Q. Shi, "Finite-element analysis of the tool tilt angle effect on the formation of friction stir welds," *Journal of Manufacturing Processes,* vol. 30, pp. 562-569, 2017.
[39] H. Robe, C. Claudin, J.-M. Bergheau, and E. Feulvarch, "R-ALE simulation of heat transfer during friction stir welding of an AA2xxx/AA7xxx joint on a large process window," *International Journal of Mechanical Sciences,* vol. 155, pp. 31-40, 2019.
[40] H. Talebi, M. Froend, and B. Klusemann, "Application of Adaptive Element-Free Galerkin Method to Simulate Friction Stir Welding of Aluminum," *Procedia Engineering,* vol. 207, pp. 580-585, 2017.
[41] N. Dialami, M. Cervera, M. Chiumenti, and C. Agelet de Saracibar, "A fast and accurate two-stage strategy to evaluate the effect of the pin tool profile on metal flow, torque and forces in friction stir welding," *International Journal of Mechanical Sciences,* vol. 122, pp. 215-227, 2017.
[42] G. Buffa, A. Ducato, and L. Fratini, "Numerical procedure for residual stresses prediction in friction stir welding," *Finite Elements in Analysis and Design,* vol. 47, no. 4, pp. 470-476, 2011.

[43] F. Al-Badour, N. Merah, A. Shuaib, and A. Bazoune, "Coupled Eulerian Lagrangian finite element modeling of friction stir welding processes," *Journal of Materials Processing Technology*, vol. 213, no. 8, pp. 1433-1439, 2013.
[44] P. Chauhan, R. Jain, S. K. Pal, and S. B. Singh, "Modeling of defects in friction stir welding using coupled Eulerian and Lagrangian method," *Journal of Manufacturing Processes*, vol. 34, pp. 158-166, 2018.
[45] K. Li, F. Jarrar, J. Sheikh-Ahmad, and F. Ozturk, "Using coupled Eulerian Lagrangian formulation for accurate modeling of the friction stir welding process," *Procedia Engineering*, vol. 207, pp. 574-579, 2017.
[46] Q. Chu, X. W. Yang, W. Y. Li, A. Vairis, and W. B. Wang, "Numerical analysis of material flow in the probeless friction stir spot welding based on Coupled Eulerian-Lagrangian approach," *Journal of Manufacturing Processes*, vol. 36, pp. 181-187, 2018.
[47] N. Dialami, M. Cervera, and M. Chiumenti, "Defect formation and material flow in Friction Stir Welding," *European Journal of Mechanics - A/Solids*, vol. 80, p. 103912, 2019.
[48] N. Mathew, I. Dinaharan, S. J. Vijay, and N. Murugan, "Microstructure and Mechanical Characterization of Aluminum Seamless Tubes Produced by Friction Stir Back Extrusion," *Transactions of the Indian Institute of Metals*, journal article vol. 69, no. 10, pp. 1811-1818, 2016.
[49] M. Sarkari Khorrami and M. Movahedi, "Microstructure evolutions and mechanical properties of tubular aluminum produced by friction stir back extrusion," *Materials and Design*, vol. 65, pp. 74-79, 2015.
[50] NASA. (Dec. 13, 2019 Accessed on: Dec. 20, 2019. [Online]). *NASA Evidence*. Available: https://climate.nasa.gov/evidence
[51] *ABAQUS User Manual*. 2013.
[52] X. Zhang, Z. Chen, and Y. Liu, "Constitutive Models," in *The Material Point Method*,Oxford: Academic Press,, 2017, pp. 175-219.
[53] *ABAQUS Theory Manual*. 2013.
[54] F. Ducobu, E. Rivière-Lorphèvre, and E. Filippi, "Mesh influence in orthogonal cutting modelling with the Coupled Eulerian-Lagrangian (CEL) method," *European Journal of Mechanics - A/Solids*, vol. 65, pp. 324-335, 2017.
[55] M. Burley, J. E. Campbell, J. Dean, and T. W. Clyne, "Johnson-Cook parameter evaluation from ballistic impact data via iterative FEM modelling," *International Journal of Impact Engineering*, vol. 112, pp. 180-192, 2018.
[56] F. Abbassi, M. Srinivasan, C. Loganathan, R. Narayanasamy, and M. Gupta, "Experimental and numerical analyses of magnesium alloy hot workability," *Journal of Magnesium and Alloys*, vol. 4, no. 4, pp. 295-301, 2016.
[57] V. Seriacopi, N. K. Fukumasu, R. M. Souza, and I. F. Machado, "Finite element analysis of the effects of thermo-mechanical loadings on a tool steel microstructure," *Engineering Failure Analysis*, vol. 97, pp. 383-398, 2019.
[58] K. Huang and R. E. Logé, "A review of dynamic recrystallization phenomena in metallic materials," *Materials & Design*, vol. 111, pp. 548-574, 2016.
[59] L. Dong, Y. Zhong, Q. Ma, C. Yuan, and L. Ma, "Dynamic Recrystallization and Grain Growth Behavior of 20SiMn Low Carbon Alloy Steel," *Tsinghua Science & Technology*, vol. 13, no. 5, pp. 609-613, 2008.
[60] C. A. C. Imbert and H. J. McQueen, "Dynamic recrystallization of A2 and M2 tool steels," *Materials Science & Engineering A*, vol. 313, no. 1, pp. 104-116, 2001.

[61] D. H. Herring, "Grain Size and Its Influence on Materials Properties," *Industrial Heating*, vol. 72, no. 8, pp. 20,22, 2005.
[62] A. Chaudhary, A. Kumar Dev, A. Goel, R. Butola, and M. S. Ranganath, "The Mechanical Properties of Different alloys in friction stir processing: A Review," *Materials Today: Proceedings: Part 1*, vol. 5, no. 2 Part 1, pp. 5553-5562, 2018.

Vita

Obadah M. Al-Jarrah was born in 1993, in Jordan. He received his primary and secondary education in Jordan. He received his B.Sc. degree in aeronautical Engineering from the Jordan University of Science and Technology in 2016.

In September 2017, he joined the Mechanical Engineering master's program in the American University of Sharjah as a graduate teaching assistant. His research interests are in experimental and computational solids mechanics and advanced materials processing.